Status of the two-Higgs-doublet model in light of the CDF m_W measurement

Soojin Lee,[1,*] Kingman Cheung,[1,2,3,†] Jinheung Kim,[1,‡] Chih-Ting Lu,[4,§] and Jeonghyeon Song[1,‖]

[1]*Department of Physics, Konkuk University, Seoul 05029, Republic of Korea*
[2]*Department of Physics, National Tsing Hwa University, Hsinchu 300, Taiwan*
[3]*Center for Theory and Computation, National Tsing Hua University, Hsinchu 300, Taiwan*
[4]*Department of Physics and Institute of Theoretical Physics, Nanjing Normal University, Nanjing 210023, China*

(Received 11 May 2022; accepted 27 September 2022; published 13 October 2022)

The most recent W-boson mass measurement by the CDF Collaboration with a substantially reduced uncertainty indicates a significant deviation from the standard model prediction, as large as 7σ if taken literally. Then the Peskin-Takeuchi parameters of S and T shift to larger values, which has profound consequences in searching for physics beyond the SM. In the framework of two-Higgs-doublet models, we study the effect of the new W-boson mass measurement on the parameter space. Combined with other constraints including theoretical requirements, flavor-changing neutral currents in B physics, the cutoff scale above 1 TeV, Higgs precision data, and direct collider search limits from the LEP, Tevatron, and LHC experiments, we find upper bounds on the masses of the heavy Higgs bosons; $M_{H,A,H^\pm} \lesssim 1.1$ TeV in type I, II, X, and Y for the normal Higgs scenario; $M_{H^\pm} \lesssim 450$ GeV and $M_A \lesssim 420$ GeV in type I and X for the inverted scenario where the heavier CP-even Higgs bosons is the observed one. Another important finding is that type II and type Y in the inverted scenario are completely excluded. Such unprecedented findings imply that the upcoming LHC run can readily close out a large portion of the, still available, parameter space.

DOI: 10.1103/PhysRevD.106.075013

I. INTRODUCTION

The standard model (SM) of electroweak theory with $SU(2) \times U(1)$ gauge symmetry is highly successful in explaining almost all the measurements in particle physics experiments. Nevertheless, we have not given up on new physics beyond the SM (BSM) to answer the outstanding questions in particle physics, such as the neutrino mass and mixing, matter-antimatter asymmetry in the Universe, and dark matter. A natural approach is to presume that a BSM theory appears at a high-energy scale while the SM is a good theory at a low-energy scale. Hence, if any experiment at the energy scale below 1 TeV observes an anomaly, it would shake the foundation on the SM and indicate the advent of a new era in particle physics.

Very recently, the CDF Collaboration at Fermilab reported the most precise W-boson mass measurement, $m_W^{\rm CDF} = 80.4335 \pm 0.0094$ GeV [1]. The total uncertainty is less than 10 MeV and the central value is about 76.5 MeV larger than the SM prediction, $m_W^{\rm SM} = 80.357 \pm 0.006$ GeV [2]. It has about 7σ standard deviation from the SM value. Before the CDF run-II result, the world average of m_W measurements had just 1.8σ standard deviations from $m_W^{\rm SM}$ [2]. Even though more careful cross-checks of the systematic uncertainties between CDF run-II analysis and other W-boson mass measurements at the LEP [3], LHCb [4], ATLAS [5], and D0 [6] will eventually be made, this new measured m_W value urgently calls for an explanation from new physics models.

An efficient parametrization to quantify the validity of the SM and to point in the direction of new physics is a set of the Peskin-Takeuchi oblique parameters of S, T, and U [7–9] in the global fit to the electroweak precision data (EWPD) [10,11]. According to Ref. [12–22], the CDF m_W yields significant deviations of the oblique parameters from the SM predictions. If all of three can vary, the new fits show that S and T can keep as before, but the U increases substantially such that $S = 0.06 \pm 0.10$, $T = 0.11 \pm 0.12$, and $U = 0.13 \pm 0.09$ [12]. Here, we take the definition of the oblique parameters which vanish in the SM [2]. However, the contributions to U can only

*soojinlee957@gmail.com
†cheung@phys.nthu.edu.tw
‡jinheung.kim1216@gmail.com
§timluyu@gmail.com
‖jhsong@konkuk.ac.kr

appear in a dimension-eight operator, so most new physics models have tiny contributions to U. Therefore, setting $U = 0$ while varying S and T is usually adopted, which results in both S and T moving to large and positive values; $S = 0.15 \pm 0.08$ and $T = 0.27 \pm 0.06$ [12]. Based on these changes of S and T, some new physics models including two-Higgs-doublet model (2HDM) and its extensions [12,23–36], the Higgs triplet model [37–41], supersymmetry [42–47], leptoquarks [48–50], seesaw mechanisms of neutrino mass [51–56], vectorlike leptons or vectorlike quarks [57–61], the standard model effective field theory (SMEFT) [14–17,19,20,62–64], and others [13,21,22,65–73] are proposed to explain the W-boson mass anomaly. In particular, some of them also try to explain the long-standing anomaly in the muon anomalous magnetic moment measurement [32,33,36,43,44,48–50,54,57,58,60], which the Fermilab has recently confirmed [74].

In this work, we pursue a comprehensive study of the 2HDM in light of the new CDF m_W measurement. We study not only four famous tree-level flavor-conserved types (type I, type II, type X, and type Y) but also two Higgs scenarios for the observed Higgs boson, the normal scenario (NS) and inverted scenario (IS). We impose all the theoretical and experimental constraints, including the stability of the scalar potential, the unitarity of the scalar-scalar scatterings, the EWPD, the Higgs precision data, and the direct search bounds at the LEP, Tevatron, and LHC. We compare the results before and after the new CDF m_W measurement. In addition, we study the evolutions of the model parameters via renormalization group equation (RGE), and demand the stability of the scalar potential up to 1 TeV. A particular focus is on a comparative study to see the differences in the viable parameter space, according to the type, Higgs scenario, and m_W. One of the most salient features when we take $m_W^{\rm CDF}$ is that the aforementioned constraints put the *upper* bounds on the masses of new Higgs bosons, about 1.1 TeV in the NS and about 450 GeV in the IS. Then type II and type Y in the IS face a conflict with the lower bound on $M_{H^\pm} \gtrsim 580$ GeV from $b \to s\gamma$ [75,76]. Consequently, type II and type Y in the IS are excluded. In addition, the results of scanning the entire parameter space without any conditions on the masses and couplings give apparent signals for the future collider phenomenologies: (i) type I has the most surviving parameter points for both NS and IS; (ii) the light charged Higgs boson at a mass below the top quark mass is viable in type I and type X; (iii) light neutral Higgs bosons, CP-even and CP-odd, are still allowed for type I and type X.

The rest of this paper is arranged as follows. We briefly review the 2HDM in Sec. II. The parameter scanning strategies are outlined in Sec. III. The allowed ranges of the masses, $\tan\beta$, and $\sin(\beta-\alpha)$ are also shown. We then discuss the characteristic features of the NS and IS in Sec. IV and Sec. V, respectively. Finally, we conclude in Sec. VI.

II. REVIEW OF 2HDM

In the 2HDM, there exist two complex $SU(2)_L$ Higgs doublet fields, Φ_1 and Φ_2 [77],

$$\Phi_i = \begin{pmatrix} w_i^+ \\ \frac{v_i + h_i + i\eta_i}{\sqrt{2}} \end{pmatrix}, \qquad i = 1, 2, \tag{1}$$

where v_1 and v_2 are the nonzero vacuum expectation values of Φ_1 and Φ_2, respectively. The electroweak symmetry is broken by $v = \sqrt{v_1^2 + v_2^2} = 246$ GeV. We define the ratio of two vacuum expectation values to be $\tan\beta = v_2/v_1$. For simplicity, we use the notation of $s_x = \sin x$, $c_x = \cos x$, and $t_x = \tan x$ in what follows.

We impose a discrete Z_2 symmetry, under which $\Phi_1 \to \Phi_1$ and $\Phi_2 \to -\Phi_2$, to avoid the flavor-changing-neutral-current (FCNC) at tree level [78,79]. The scalar potential with CP invariance and softly broken Z_2 is

$$\begin{aligned} V = {} & m_{11}^2 \Phi_1^\dagger \Phi_1 + m_{22}^2 \Phi_2^\dagger \Phi_2 - m_{12}^2 (\Phi_1^\dagger \Phi_2 + \text{H.c.}) \\ & + \frac{1}{2}\lambda_1 (\Phi_1^\dagger \Phi_1)^2 + \frac{1}{2}\lambda_2 (\Phi_2^\dagger \Phi_2)^2 + \lambda_3 (\Phi_1^\dagger \Phi_1)(\Phi_2^\dagger \Phi_2) \\ & + \lambda_4 (\Phi_1^\dagger \Phi_2)(\Phi_2^\dagger \Phi_1) + \frac{1}{2}\lambda_5 [(\Phi_1^\dagger \Phi_2)^2 + \text{H.c.}], \end{aligned} \tag{2}$$

where the m_{12}^2 term softly breaks the Z_2 parity. The model has five physical Higgs bosons, the lighter CP-even scalar h, the heavier CP-even scalar H, the CP-odd pseudoscalar A, and a pair of charged Higgs bosons $H^\pm$. The weak eigenstates in Eq. (1) are linear combinations of physical Higgs bosons through two mixing angles, α and β: the expressions are referred to Ref. [80]. An important relationship is the SM Higgs boson $h_{\rm SM}$ with h and H,

$$h_{\rm SM} = s_{\beta-\alpha} h + c_{\beta-\alpha} H. \tag{3}$$

In the 2HDM, the observed Higgs boson at a mass of 125 GeV can be either h or H, which is called the normal scenario (NS) and the inverted scenario (IS) [81,82], respectively,

$$\begin{aligned} &\text{NS:}\ m_h = m_{125}; \\ &\text{IS:}\ M_H = m_{125}, \end{aligned} \tag{4}$$

where $m_{125} = 125$ GeV. A popular way to accommodate the SM-like Higgs boson is the Higgs alignment limit where $h_{\rm SM} = h$ (or $c_{\beta-\alpha} = 0$) in the NS and $h_{\rm SM} = H$ (or $s_{\beta-\alpha} = 0$) in the IS. Then the phenomenology of the BSM Higgs bosons is simplified such that $H \to WW/ZZ$, $A \to Zh_{\rm SM}$, and $H^\pm \to W^{\pm(*)} h_{\rm SM}$ are prohibited at tree level. However, the assumption may interfere with observing new scalar bosons at the LHC. Therefore, we do not impose any conditions on the masses and couplings when

performing the random scan. Only the theoretical and experimental constraints will restrict the parameter space.

We take six free parameters of

$$\{m_h, \quad M_{H^\pm}, \quad M_H, \quad M_A, \quad m_{12}^2, \quad t_\beta, \quad s_{\beta-\alpha}\}. \tag{5}$$

The range of $(\beta-\alpha)$ is set to be $[-\pi/2, \pi/2]$, as in the public codes of 2HDMC [83], HIGGSSIGNALS [84], and HIGGSBOUNDS [85]. The quartic couplings are [86]

$$\begin{aligned}
\lambda_1 &= \frac{1}{v^2 c_\beta^2}[c_\alpha^2 M_H^2 + s_\alpha^2 m_h^2 - s_\beta^2 M^2], \\
\lambda_2 &= \frac{1}{v^2 s_\beta^2}[s_\alpha^2 M_H^2 + c_\alpha^2 m_h^2 - c_\beta^2 M^2], \\
\lambda_3 &= \frac{1}{v^2}\left[2M_{H^\pm}^2 + \frac{s_{2\alpha}}{s_{2\beta}}(M_H^2 - m_h^2) - M^2\right], \\
\lambda_4 &= \frac{1}{v^2}[M_A^2 - 2M_{H^\pm}^2 + M^2], \\
\lambda_5 &= \frac{1}{v^2}[M^2 - M_A^2],
\end{aligned} \tag{6}$$

where $M^2 = m_{12}^2/(s_\beta c_\beta)$.

According to the Z_2 parity of the fermion singlets, there are four types in the 2HDM, type I, type II, type X, and type Y, which have different Yukawa couplings of the SM fermions. We parametrize the Yukawa Lagrangian as

$$\begin{aligned}
\mathscr{L}_{\rm Yuk} = &-\sum_f \left(\frac{m_f}{v}\xi_f^h \bar{f} f h + \frac{m_f}{v}\xi_f^H \bar{f} f H - i\frac{m_f}{v}\xi_f^A \bar{f}\gamma_5 f A\right) \\
&- \left\{\frac{\sqrt{2}V_{ud}}{v} H^+ \bar{u}(m_u \xi_u^A \mathrm{P}_L + m_d \xi_d^A \mathrm{P}_R) d \right. \\
&\left. + \frac{\sqrt{2}m_\ell}{v} H^+ \xi_\ell^A \bar{\nu}_L \ell_R + \text{H.c.}\right\},
\end{aligned} \tag{7}$$

where $\xi_f^{h,H,A}$ are presented in Table I. To specify the eight cases (four types in the NS and four types in the IS), we shall sometimes use a simplified name; for instance, NS-I denotes type I in the NS.

Now let us get into the comparative study in the 2HDM before and after the CDF m_W measurement, denoted by the "PDG" and "CDF" cases, respectively. The Peskin-Takeuchi oblique parameters with $U = 0$ in two cases are

$$S_{\rm PDG} = 0.05 \pm 0.08, \quad T_{\rm PDG} = 0.09 \pm 0.07, \quad \rho_{\rm PDG} = 0.92, \tag{8}$$

$$S_{\rm CDF} = 0.15 \pm 0.08, \quad T_{\rm CDF} = 0.27 \pm 0.06, \quad \rho_{\rm CDF} = 0.93, \tag{9}$$

where ρ is the correlation between S and T.

TABLE I. The Yukawa coupling modifiers in four types of the 2HDM.

	ξ_u^h	ξ_d^h	ξ_ℓ^h	ξ_u^H	ξ_d^H	ξ_ℓ^H	ξ_u^A	ξ_d^A	ξ_ℓ^A
Type I	$\frac{c_\alpha}{s_\beta}$	$\frac{c_\alpha}{s_\beta}$	$\frac{c_\alpha}{s_\beta}$	$\frac{s_\alpha}{s_\beta}$	$\frac{s_\alpha}{s_\beta}$	$\frac{s_\alpha}{s_\beta}$	$\frac{1}{t_\beta}$	$-\frac{1}{t_\beta}$	$-\frac{1}{t_\beta}$
Type II	$\frac{c_\alpha}{s_\beta}$	$-\frac{s_\alpha}{c_\beta}$	$-\frac{s_\alpha}{c_\beta}$	$\frac{s_\alpha}{s_\beta}$	$\frac{c_\alpha}{c_\beta}$	$\frac{c_\alpha}{c_\beta}$	$\frac{1}{t_\beta}$	t_β	t_β
Type X	$\frac{c_\alpha}{s_\beta}$	$\frac{c_\alpha}{s_\beta}$	$-\frac{s_\alpha}{c_\beta}$	$\frac{s_\alpha}{s_\beta}$	$\frac{s_\alpha}{s_\beta}$	$\frac{c_\alpha}{c_\beta}$	$\frac{1}{t_\beta}$	$-\frac{1}{t_\beta}$	t_β
Type Y	$\frac{c_\alpha}{s_\beta}$	$-\frac{s_\alpha}{c_\beta}$	$\frac{c_\alpha}{s_\beta}$	$\frac{s_\alpha}{s_\beta}$	$\frac{c_\alpha}{c_\beta}$	$\frac{s_\alpha}{s_\beta}$	$\frac{1}{t_\beta}$	t_β	$-\frac{1}{t_\beta}$

The biggest difference between the PDG and CDF cases is that the CDF m_W does not allow new Higgs bosons heavier than about 1.1 TeV, while the PDG allows, which will be explicitly shown in the next section. To reveal the origin of this key feature, let us consider heavy charged Higgs bosons with $M_{H^\pm} = 1.5$ TeV. For simplicity, we concentrate on the NS in the Higgs alignment limit ($s_{\beta-\alpha} = 1$), where the quartic couplings are

$$\begin{aligned}
\lambda_1^{\rm NS-Al} &= \frac{1}{v^2}[t_\beta^2(M_H^2 - M^2) - m_h^2], \\
\lambda_2^{\rm NS-Al} &= \frac{1}{v^2}\left[m_h^2 + \frac{1}{t_\beta^2}(M_H^2 - M^2)\right], \\
\lambda_3^{\rm NS-Al} &= \frac{1}{v^2}[m_h^2 + 2M_{H^\pm}^2 - M_H^2 - M^2].
\end{aligned} \tag{10}$$

$\lambda_4^{\rm NS-Al}$ and $\lambda_5^{\rm NS-Al}$ are the same as in (6). It is well known in the literature [86–98] that if any quartic coupling at the electroweak scale is not small enough, its magnitude grows rapidly as the energy scale increases, ending up with the breaking of the stability of the scalar potential. For illustration purposes, let us select λ_3 among five quartic couplings because it is independent of t_β but sensitive to three new masses.[1] Figure 1 shows $(\Delta M_H, \Delta M_A)$ with $M^2 = M_A^2$, allowed by S and T at 1σ level (red), at 2σ level (yellow), $|\lambda_3| < 4\pi$ (light blue), and $|\lambda_3| < 2\pi$ (green). Here $\Delta M_{H,A}$ is defined by

$$\Delta M_{H,A} \equiv M_{H,A} - M_{H^\pm}. \tag{11}$$

The PDG result is in the left panel, and the CDF result is in the right panel. The condition of $|\lambda_3| < 4\pi$ is for the perturbativity of the quartic coupling, and $|\lambda_3| < 2\pi$ is for $\Lambda_c > 1$ TeV; the bound of 2π is chosen because it is the maximum of $|\lambda_3|$ allowed by $\Lambda_c > 1$ TeV in the full RGE analysis.

Figure 1 clearly shows the difference between the PDG and CDF cases. First, the oblique parameters allow $M_{H^\pm} = M_H = M_A$ in the PDG case, but not in the CDF case. Notice that heavy masses of new Higgs bosons are still

[1] In the next section, we will perform the complete RGE analysis for the gauge, Yukawa, and quartic couplings.

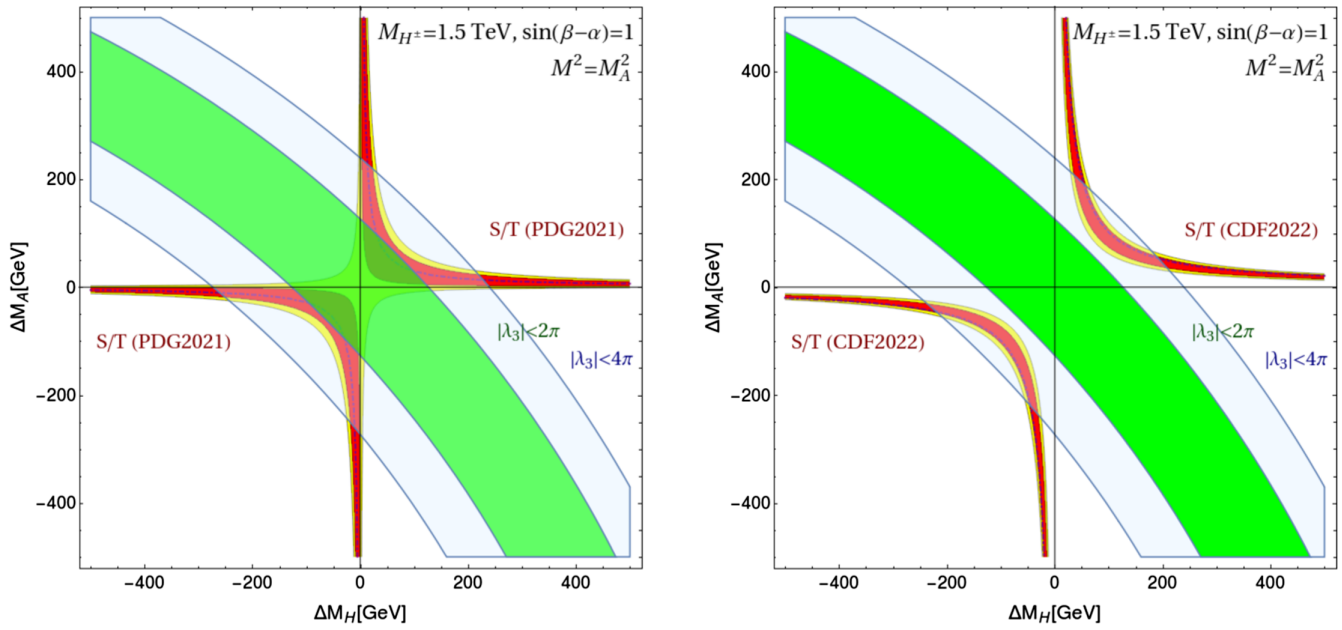

FIG. 1. Allowed regions of $(\Delta M_H, \Delta M_A)$ by the oblique parameters of S and T (red at 1σ and yellow in 2σ), $|\lambda_3| < 4\pi$ (light blue), and $|\lambda_3| < 2\pi$ (green), where $\Delta M_{H,A} \equiv M_{H,A} - M_{H^\pm}$. The left (right) panel shows the PDG (CDF) results. We set $M_{H^\pm} = 1.5$ TeV and $M^2 = M_A^2$ in the normal scenario with $s_{\beta-\alpha} = 1$.

consistent with $T_{\rm CDF}$ in Eq. (9); for example, very heavy M_A is feasible if $\Delta M_H \simeq 0$. When applying the perturbativity of $|\lambda_3| < 4\pi$ (light blue), however, large mass gaps of ΔM_H and ΔM_A are forbidden in both cases. When narrowing the range further into $|\lambda_3| < 2\pi$ for $\Lambda_c > 1$ TeV, there is no overlap in the CDF case. Thus, heavy Higgs bosons cannot simultaneously satisfy $T_{\rm CDF}$ and $\Lambda_c > 1$ TeV. For lighter $M_{H^\pm}$, however, the CDF case also permits an overlap because of Eq. (10).

III. SCANNING STRATEGIES AND THE RESULTS

We perform random scanning of the model parameters by imposing all the theoretical and experimental constraints. The scanning ranges in the NS and IS are

$$\begin{aligned}
&\text{NS}: M_H \in [130, 2000]\ \text{GeV}, \quad M_A \in [15, 2000]\ \text{GeV},\\
&\quad |s_{\beta-\alpha}| \in [0.8, 1.0], \quad m_{12}^2 \in [0, 1000^2]\ \text{GeV}^2,\\
&\text{IS}: m_h \in [15, 120]\ \text{GeV}, \quad M_A \in [15, 2000]\ \text{GeV},\\
&\quad |s_{\beta-\alpha}| \in [0, 0.6], \quad m_{12}^2 \in [0, 1000^2]\ \text{GeV}^2. \qquad (12)
\end{aligned}$$

For the FCNC observables [75,76], we take different ranges of $M_{H^\pm}$ and t_β for type I/X and type II/Y:

$$\begin{aligned}
&\text{type I/X}: M_{H^\pm} \in [80, 2000]\ \text{GeV}, \quad t_\beta \in [1, 50],\\
&\text{type II/Y}: M_{H^\pm} \in [580, 2000]\ \text{GeV}, \quad t_\beta \in [0.5, 50]. \qquad (13)
\end{aligned}$$

The range of $s_{\beta-\alpha}$ is motivated by the current Higgs precision data [99]. And we scan over positive m_{12}^2 because we found in the preliminary scanning that a parameter point with negative m_{12}^2 does not satisfy the perturbativity, unitarity, or vacuum stability. It is evident in λ_1; see Eq. (10). If $m_{12}^2 < 0$, the terms proportional to t_β^2 yield large $|\lambda_1|$ and thus threaten the perturbativity, especially for large t_β. In the preliminary check, we found that the vacuum stability condition is the most crucial factor in excluding the parameter points with negative m_{12}^2. If $m_{12}^2 > 0$, however, the contribution from M^2 cancels that from M_H^2. For more efficient scanning, therefore, only the positive values of m_{12}^2 are considered.

We randomly generate the six-dimensional parameter points in Eqs. (12) and (13), which are uniformly distributed. Over the generated parameter points, we cumulatively impose the following steps:

Step (i) Theory+FCNC: We require a parameter point to satisfy the theoretical stabilities and the FCNC results using the public code 2HDMC-v1.8.0 [83].

(1) Higgs potential being bounded from below [100];
(2) Perturbative unitarity of the amplitudes of scalar-scalar, scalar-vector, and vector-vector scatterings at high energies [101,102];
(3) Perturbativity of the quartic couplings [77,81];
(4) Vacuum stability [103];
(5) FCNC observables [75,76,104].

Step (ii) EWPD: We calculate the Peskin-Takeuchi oblique parameters of S and T in the 2HDM [105–107], and

compare them with the PDG and CDF results in Eqs. (8) and (9). For two-parameter fitting under the assumption of $U = 0$, we require $\chi^2 < 5.99$ which corresponds to $p > 0.05$.

Step (iii) RGEs for $\Lambda_c > 1$ TeV: We demand that the cutoff scale should be larger than 1 TeV. Using the RGE in the 2HDM [77,86,95,108,109], we run the gauge couplings, the quartic couplings in the scalar potential, and the Yukawa couplings of the top quark, bottom quark, and tau lepton. The initial conditions of the gauge couplings and the Yukawa couplings are set at the top quark mass scale $m_t = 173.34$ GeV [110]. We check the perturbativity, unitarity, and vacuum stability as we increase the energy scale. If any condition is broken at the energy scale below 1 TeV, we discard the parameter point. We use the public code 2HDME-v1.2 [110] at one-loop level.

Step (iv) Collider: The collider constraints consist of two categories, the Higgs precision data and the direct search bounds at the LEP, Tevatron, and LHC. To check the consistency with the Higgs precision data, we use HIGGSSIGNALS-v2.6.2 [84], which yields the χ^2 output for 111 Higgs observables [111–118]. Since there are six model parameters, the number of degrees of freedom is 105. We demand that the p-value be larger than 0.05. For a consistency check with the direct searches at high-energy colliders, we use the public code HIGGSBOUNDS-v5.10.2 [85]. For each process, we calculate the cross section in the model. When the model prediction is larger than the observed upper bound at 95% CL, we rule out the parameter point.

For each type in the NS and IS, we obtained 10^7 parameter points that satisfy Step (i), which required to generate more than 10^{10} parameter points. Before proceeding to the subsequent steps, let us investigate the implications of Step (i). In Fig. 2, we present M_A versus M_H after Step-(i), where the color codes denote $M_{H^\pm}$. The results in the NS (IS) are in the upper (lower) panels, and those at type I/X

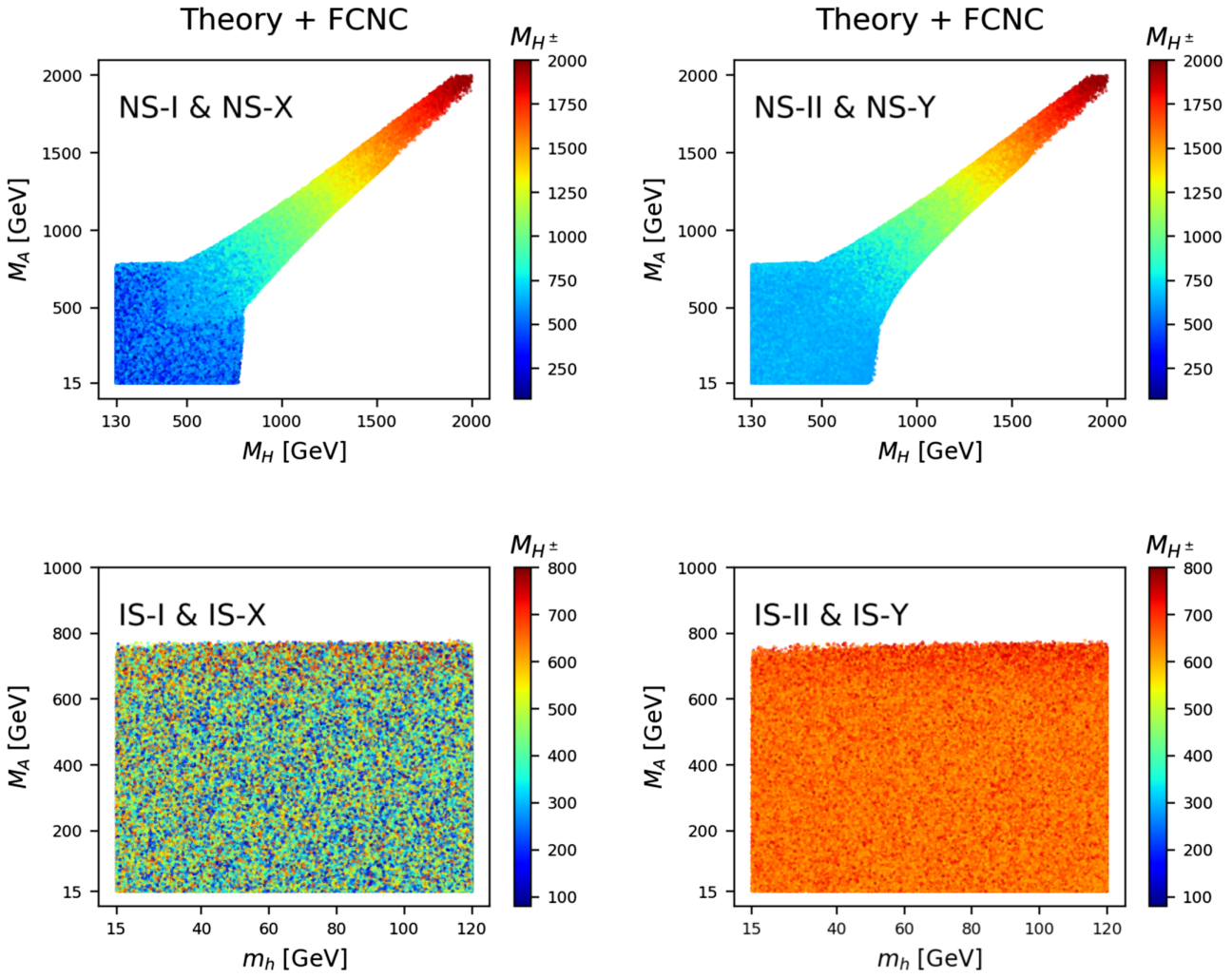

FIG. 2. Allowed regions of (M_H, M_A) in the NS (upper panels) and (m_h, M_A) in the IS (lower panels) by the theoretical requirements and the FCNC observables. The results in type I and type X are in the left panels, while those in type II and type Y are in the right panels. The color codes indicate $M_{H^\pm}$.

TABLE II. The numbers of the parameter points that survive each step in the NS and IS for all the four types. We linearly scan the parameters in Eqs. (12) and (13). For the EWPD, we adopt two different schemes of the oblique parameters, without and with the CDF-updated m_W measurement, denoted by "PDG" and "CDF".

		Theory	EWPD	RGE	Collider	Theory	EWPD	RGE	Collider
Type		Normal scenario				Inverted scenario			
I	PDG	10^7	1.3×10^6	5.1×10^5	6.0×10^4	10^7	7.2×10^5	5.1×10^5	8.5×10^4
	CDF	10^7	4.4×10^5	1.3×10^5	1.4×10^4	10^7	1.3×10^5	7.2×10^4	1.9×10^4
II	PDG	10^7	1.1×10^6	4.3×10^4	2.0×10^4	10^7	2.1×10^5	0	0
	CDF	10^7	3.4×10^5	3.0×10^3	1.0×10^3	10^7	6.9×10^4	0	0
X	PDG	10^7	1.3×10^6	5.1×10^5	1.8×10^4	10^7	7.2×10^5	5.1×10^5	3.0×10^3
	CDF	10^7	4.4×10^5	1.3×10^5	3.0×10^3	10^7	1.3×10^5	7.2×10^4	1.0×10^3
Y	PDG	10^7	1.1×10^6	4.3×10^4	2.0×10^4	10^7	2.1×10^5	0	0
	CDF	10^7	3.4×10^5	3.0×10^3	1.0×10^3	10^7	6.9×10^4	0	0

(type II/Y) are in the left (right) panels. Figure 2 obviously illustrates that the theoretical requirements and the FCNC observables significantly restrict the masses of new Higgs bosons. In the NS, Step (i) demands very similar masses of new Higgs bosons in the high-mass region of $M_{A,H,H^\pm} \gtrsim 750$ GeV, while the low mass regions are uniformly permitted without correlations among the masses. In the IS, Step (i) already puts the upper bounds on M_A and $M_{H^\pm}$, below about 750 GeV.

Now, we cumulatively impose the constraints of Step (ii), Step (iii), and Step (iv). In Table II, we present the number of the parameter points that pass each step in the sixteen cases, the four types in the NS and IS without and with the CDF m_W measurement. We are well aware that just because a model has more surviving parameter points does not mean it is superior; nature takes only one parameter point. Nonetheless, the study of the surviving percentages is meaningful in the situation where the experimentalists make every effort to find a new signal without any information. A model with more allowed parameter points leaves more room for experimental exploration. In addition, it is very important to present which constraint excludes which model more severely. The bottom line is that the results in Table II provide the immediate comparison of 16 cases, coming to the main conclusions; type I has the most surviving parameter points,and type II and type Y in the IS are excluded.

Brief comments on the dependence of the survival percentages on the scanning procedure are in order here. We took the uniformly distributed samples over $M_{H^\pm}$, M_A, $M_{H/h}$, $s_{\beta-\alpha}$, t_β, and m_{12}^2. If the sampling were different, the results in Table II would be different. To estimate the changes, we randomly scan over m_{12}, instead of m_{12}^2. Scanning over $\log(m)$ is inappropriate since the upper bounds on the masses are only about 1 TeV. The changes are below 10% for type I/X and of the order of 10% for type II/Y. Consequently, the numbers in Table II are not physical, yet provide fair comparisons among all 16 cases. However, the changes are not big enough to overturn the main conclusions in the comparative study of 16 cases, such that type I has more parameter points than type X. So, we discuss the physical implications of the CDF m_W measurement, based on the sampling over Eq. (12) and (13).

Let us compare the overall differences between the NS and IS. In the NS, all the types pass the final Step (iv). We find that type I has the most parameter points survived, while type II and type Y have the fewest. In the IS, type II and type Y are excluded both in the PDG and CDF cases.[2] Decisive is the combination of $\Lambda_c > 1$ TeV and the FCNC observables. Since the former demands similar mass scales of the BSM Higgs bosons, the light mass of m_h, below 125 GeV by definition, necessitates light $M_{H^\pm}$. Then the condition of $M_{H^\pm} > 580$ GeV from $b \to s\gamma$ prohibits the model. Type I and type X, on the other hand, can accommodate the light charged Higgs boson without conflicting the FCNC observables. So they are still allowed in the IS.

Now we discuss the differences between the PDG and CDF cases. The CDF m_W allows fewer parameter points regardless of the type or the Higgs scenario; the survival percentages are of the order of 0.01% for the CDF, but of the order of 0.1% for the PDG result. The difference becomes evident from Step (ii). It is due to the tension that the EWPD needs sizable mass gaps in the CDF case but $\Lambda_c > 1$ TeV favors the mass degeneracy [86]. To demonstrate this feature in more detail, we present M_A versus M_H at each step for the NS-I in Fig. 3. The upper (lower) panels present the results for the PDG (CDF) case, and the results after Step (ii), Step (iii), and Step (iv) are in the left, middle, and right panels, respectively. At Step (ii), the PDG and

[2]We confirmed this conclusion by increasing the number of points in random scanning.

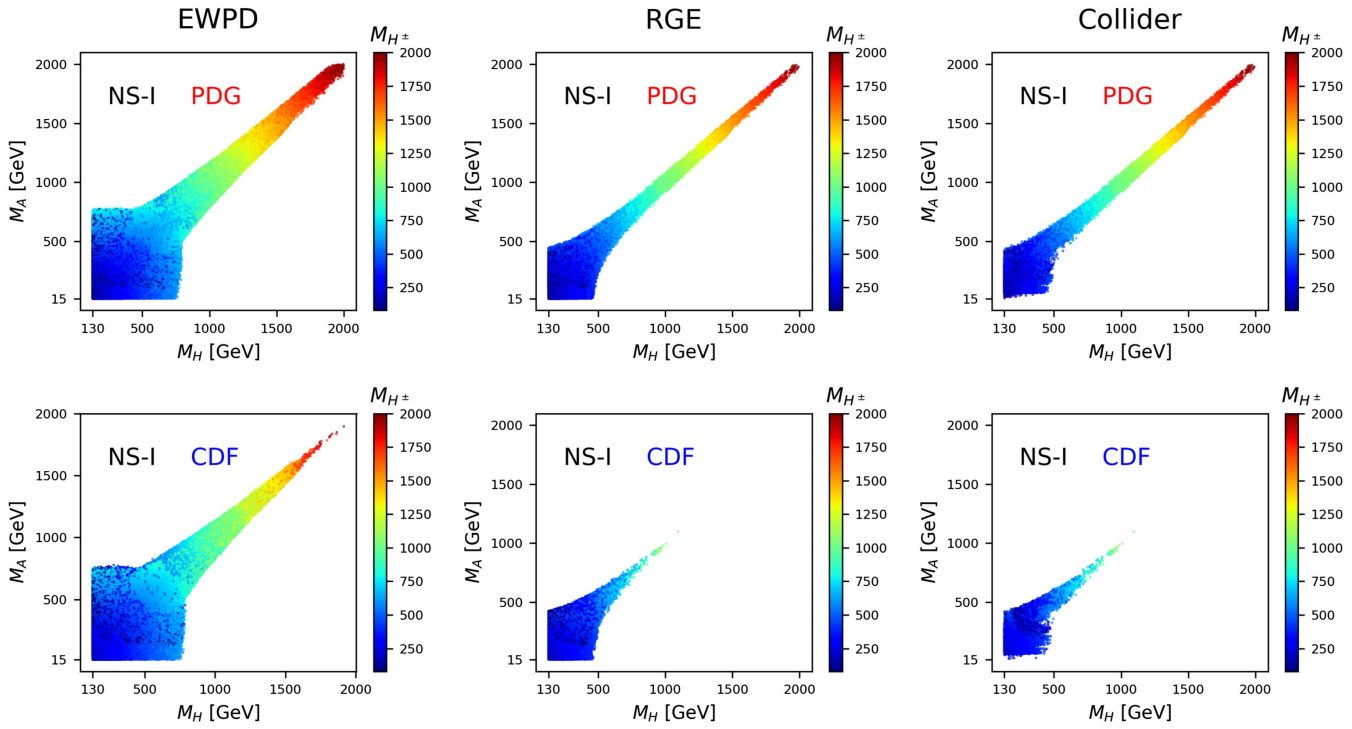

FIG. 3. In type I of the normal scenario, the allowed parameter space of (M_H, M_A) after Step (ii) (EWPD), Step (iii) (Step (ii)+RGE), and Step (iv) (Step(iii) + Higgs precision + Direct searches), with the color code indicating $M_{H^\pm}$. The upper panels are for PDG and the lower panels for CDF.

CDF cases yield similar funnel shapes in (M_H, M_A), stretching to the heavy mass regions. However, the size is different—the CDF case permits a slimmer area with substantial mass gaps. When imposing $\Lambda_c > 1$ TeV at Step (iii), the difference between the PDG and CDF is stark. The heavy mass region is excluded in the CDF case as discussed in Fig. 1. In summary, the combination of the S/T constraint with $\Lambda_c > 1$ TeV puts the upper bounds on the masses of new Higgs bosons in the CDF case. Step (iv) including the Higgs precision data and the direct search bounds also reduces the parameter space, both in the PDG and CDF cases.

Figure 4 presents the same results of M_A versus M_H for type II. As in type I, the EWPD yield similar shapes in (M_H, M_A) for the PDG and CDF cases, and $\Lambda_c > 1$ TeV at Step (iii) puts the upper bounds on the masses of new Higgs bosons only in the CDF case. Contrary to type I, $\Lambda_c > 1$ TeV also places the lower bounds on M_H and M_A above about 580 GeV both in the PDG and CDF cases. It is attributed to the combination of $M_{H^\pm} \gtrsim 580$ GeV by $b \to s\gamma$ with the similar mass scales of the BSM Higgs bosons by $\Lambda_c > 1$ TeV. At the final Step (iv), many parameter points are further excluded, but the mass bounds of new Higgs bosons remain almost intact.

The upper bounds on the new Higgs boson masses in the CDF case have profound implications in the searches at the HL-LHC. So, we present the allowed mass ranges in the CDF case for the NS

$$\begin{aligned}
&\text{NS-I: } M_{H^\pm} \in [87, 1091]\ \text{GeV},\\
&\qquad M_H \in [130, 1092]\ \text{GeV}, \quad M_A \in [22, 1098]\ \text{GeV};\\
&\text{NS-II: } M_{H^\pm} \in [598, 1139]\ \text{GeV},\\
&\qquad M_H \in [419, 1128]\ \text{GeV}, \quad M_A \in [459, 1125]\ \text{GeV};\\
&\text{NS-X: } M_{H^\pm} \in [99, 1091]\ \text{GeV},\\
&\qquad M_H \in [132, 1092]\ \text{GeV}, \quad M_A \in [30, 1098]\ \text{GeV};\\
&\text{NS-Y: } M_{H^\pm} \in [595, 1139]\ \text{GeV},\\
&\qquad M_H \in [419, 1128]\ \text{GeV}, \quad M_A \in [459, 1125]\ \text{GeV};
\end{aligned} \tag{14}$$

and for the IS

$$\begin{aligned}
&\text{IS-I: } M_{H^\pm} \in [144, 455]\ \text{GeV},\\
&\qquad M_H \in [16, 120]\ \text{GeV}, \quad M_A \in [38, 429]\ \text{GeV};\\
&\text{IS-X: } M_{H^\pm} \in [166, 446]\ \text{GeV},\\
&\qquad M_H \in [62.5, 120]\ \text{GeV}, \quad M_A \in [16, 420]\ \text{GeV}.
\end{aligned} \tag{15}$$

Finally, we want to discuss the possibility of light BSM Higgs bosons in the CDF case. First, a light charged Higgs boson with a mass below the top quark mass is feasible in type I and type X. It is consistent with the current searches

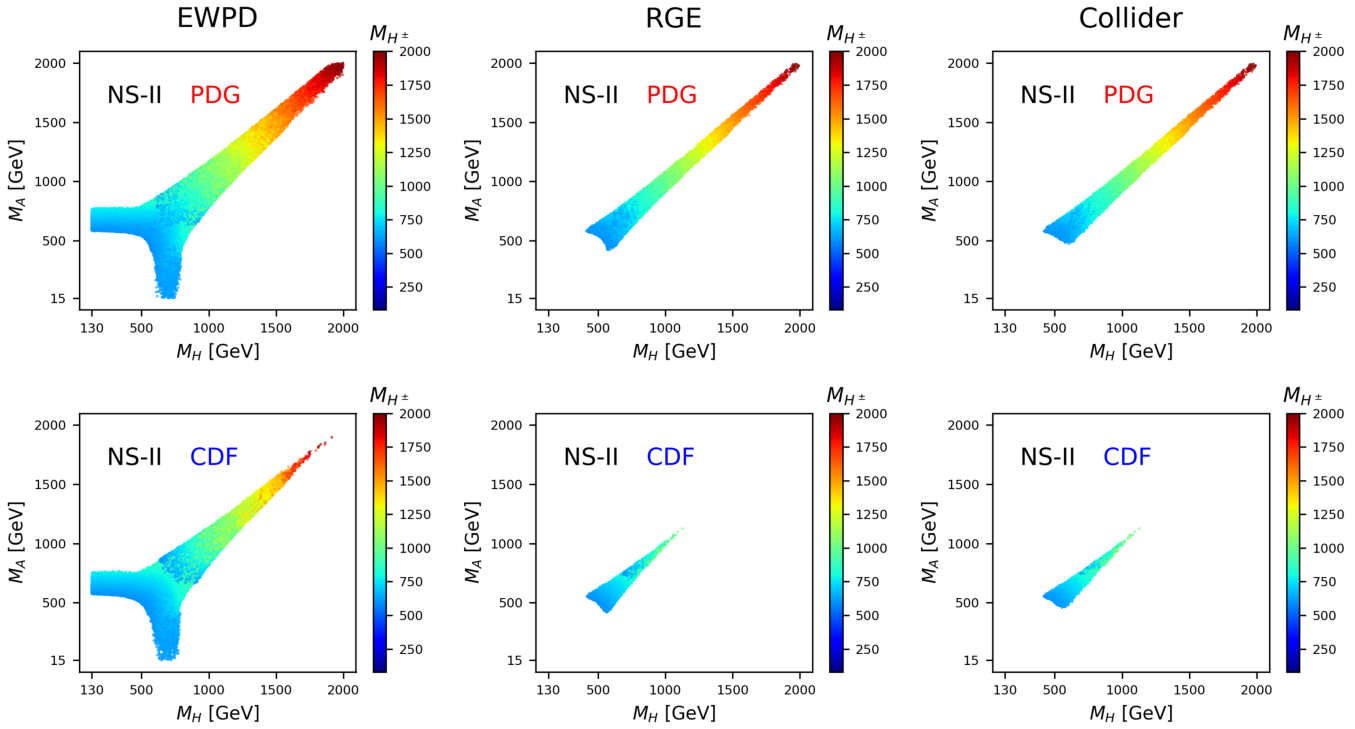

FIG. 4. In type II of the normal scenario, the allowed parameter space of (M_H, M_A) after Step (ii), Step (iii), and Step (iv), with the color code indicating $M_{H^\pm}$. The upper panels are for PDG while the lower panels for CDF.

for the light charged Higgs boson at the LHC via the production of $t \to H^\pm b$ in the decay modes of $H^\pm \to \tau^\pm \nu$ [119,120], $H^\pm \to cb$ [121,122], and $H^\pm \to cs$ [123–125]. For future searches, the detailed characteristics of the light $H^\pm$ is important. In the IS, the mass difference of the light $M_{H^\pm}$ from the top quark mass is small [see Eq. (15)]. The soft b jet in the process of $t \to H^\pm b$ makes it challenging to observe the light $H^\pm$ through the conventional production channel [126,127]. Bosonic productions of the light charged Higgs boson are more efficient in this case [128]. In the NS, type I and type X accommodate a larger mass gap between m_t and $M_{H^\pm}$ but the b jet from $t \to H^\pm b$ is still too soft to enjoy high b-tagging efficiency.

Second, a light pseudoscalar at a mass below 62.5 GeV is allowed in type I and type X. Although it seems to contradict the current data on the exotic Higgs decay of $h_{\rm SM} \to AA$, the final parameter points pass the HIGGSSIGNALS and HIGGSBOUNDS, especially the CMS searches for $h_{\rm SM} \to AA$ in the final states of $2\mu 2\tau/4\tau$ [129], $4\tau/2\mu 2b/2\mu 2\tau$ [130], and $2\mu 2\tau$ [131], as well as the LEP search for $e^+e^- \to 4bZ/4\tau Z$ [132]. The main reason is small trilinear coupling $\hat{\lambda}_{hAA}$, which is defined by $\mathscr{L} \supset (1/2)v\hat{\lambda}_{hAA}h_{\rm SM}AA$. In the NS, $\hat{\lambda}_{hAA}$ is [36]

$$\hat{\lambda}^{\rm NS}_{hAA} = (2M^2 - 2M_A^2 - m_h^2)s_{\beta-\alpha} + (m_h^2 - M^2)\left(t_\beta - \frac{1}{t_\beta}\right)c_{\beta-\alpha}. \tag{16}$$

If $M^2 \simeq M_A^2 + m_h^2/2$, $\hat{\lambda}_{hAA}$ and thus $\mathrm{Br}(h_{\rm SM} \to AA)$ are suppressed. We found that the finally allowed parameters accommodate $\mathrm{Br}(h_{\rm SM} \to AA) \lesssim 0.22$ in type I and $\mathrm{Br}(h_{\rm SM} \to AA) \lesssim 0.11$ in type X. Larger $\mathrm{Br}(h_{\rm SM} \to AA)$ in type I is explained by the dominant decay of $A \to bb$ with the branching ratio of about 80%, which invalidates the main search modes of $A \to 2\tau/2\mu$.

IV. CHARACTERISTIC FEATURES OF THE NORMAL SCENARIO

In this section we study the characteristics of the finally allowed parameter points in the NS. Since the results of type I (type II) are similar to those of type X (type Y), we show type I and type X (type II and type Y) together.

A. Type I and type X

To take a closer look at the allowed masses of the BSM Higgs bosons at the final Step (iv), we present M_A versus M_H with a color code of $M_{H^\pm}$ for type I (left panel) and type X (right panel) in Fig. 5. In the heavy mass region with $M_{H,A} \gtrsim 600$ GeV, a correlation exists among the masses of new Higgs bosons. Both ΔM_H and ΔM_A are clustered around $\Delta M_{H,A} \simeq -100$ GeV. For $M_{H,A} \lesssim 600$ GeV, the mass correlations are weak.

Now we move on to the couplings. Figure 6 presents t_β versus $|s_{\beta-\alpha}|$ in type I (upper panels) and type X (lower panels), with a color code indicating $M_{H^\pm}$. We compare the results in the PDG case (left panels) with those in the CDF

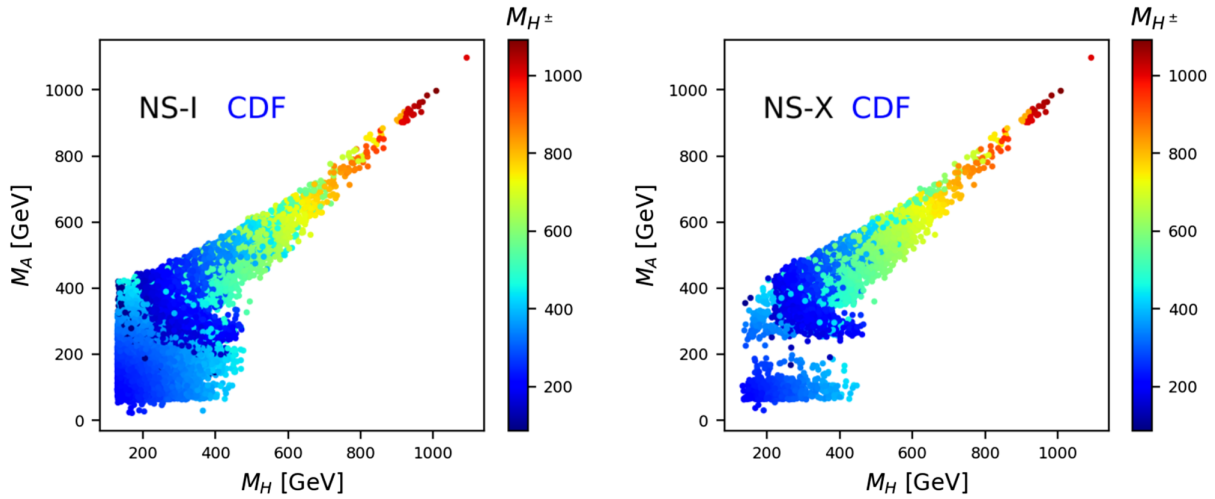

FIG. 5. M_A versus M_H with a color code of $M_{H^\pm}$ in type I (left panel) and type X (right panel) in the CDF case. We focus on the normal scenario.

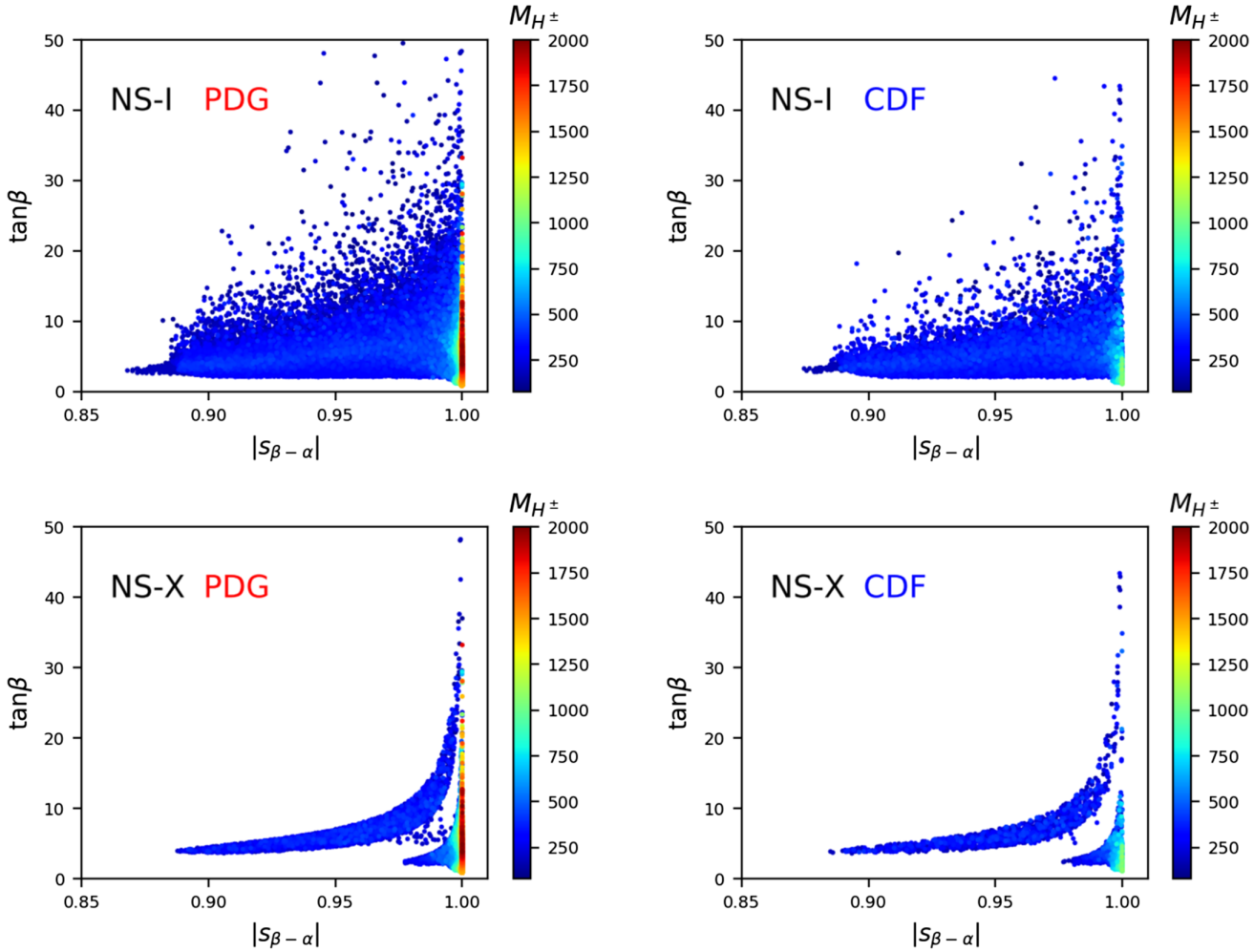

FIG. 6. Allowed regions of $(|s_{\beta-\alpha}|, t_\beta)$ in type I (upper panels) and type X (lower panels), with a color code indicating $M_{H^\pm}$ for the normal scenario. We compare the results before (left panels) and after (right panels) the CDF m_W measurement.

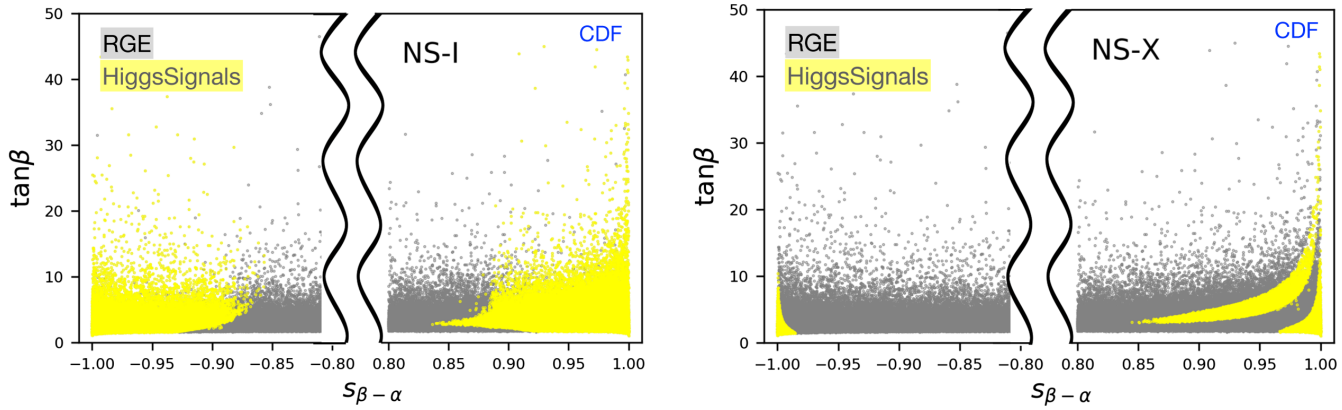

FIG. 7. t_β versus $s_{\beta-\alpha}$ in type I (left panel) and type X (right panel) of the normal scenario that pass the RGE (gray) and the Higgs precision data (yellow).

case (right panels). The Higgs precision data play a vital role in limiting $|s_{\beta-\alpha}| \gtrsim 0.88$ at 95% CL, which is similar in all the four panels. But the distributions of t_β are noticeably different according to the type and m_W. In type I, t_β is more spread out than in type X. Inside type I, the PDG and CDF show dissimilar patterns; t_β in the CDF case is clustered in smaller value region than in the PDG case. Since all the fermion Yukawa couplings to H, A, and $H^\pm$ in type I are inversely proportional to t_β in the Higgs alignment limit, small t_β increases the LHC discovery potential of new Higgs bosons through fermionic production and decay channels. In type X, a correlation between t_β and $|s_{\beta-\alpha}|$ is strong. There exists an upper bound on t_β when the Higgs alignment is broken even a little, for instance, $t_\beta < 7$ if $|s_{\beta-\alpha}| = 0.95$.

Another observation in Fig. 6 is the "arm" region in type X. It is due to the different effects of the Higgs precision data on the positive and negative $s_{\beta-\alpha}$ regions.[3] In Fig. 7 we separately display, over $(|s_{\beta-\alpha}|, t_\beta)$, the parameter points with $\Lambda_c > 1$ TeV (gray) and those additionally satisfying the Higgs precision data (yellow); yellow points are on top of gray ones. The results of NS-I are in the left panel and those of NS-X are in the right panel. At Step (iii) with the RGE analysis, the allowed region for $s_{\beta-\alpha}$ is almost symmetric about $s_{\beta-\alpha} = 0$. When imposing the Higgs precision data, type I keeps the symmetric shape but type X does not. In type X, most of the parameter space with negative $s_{\beta-\alpha}$ is excluded, except for the Higgs alignment limit.

The presence or absence of the arm region is determined by the tau lepton Yukawa coupling to the Higgs boson h,

$$\text{NS-I: } \xi_\tau^h = \frac{c_\alpha}{s_\beta} = s_{\beta-\alpha} + \frac{c_{\beta-\alpha}}{t_\beta}, \tag{17}$$

$$\text{NS-X: } \xi_\tau^h = -\frac{s_\alpha}{c_\beta} = s_{\beta-\alpha} - t_\beta c_{\beta-\alpha}. \tag{18}$$

In type I, the $c_{\beta-\alpha}$ term is suppressed by large t_β so $s_{\beta-\alpha} \simeq -1$ does not change $|\xi_\tau^h|$ much. This is why negative $s_{\beta-\alpha}$ satisfies the Higgs precision data in type I. In type X, however, the $c_{\beta-\alpha}$ term is proportional to t_β. If $s_{\beta-\alpha} = -1 + \epsilon$ and $\epsilon \neq 0$, large enough t_β overly increases $|\xi_\tau^h|$ so that the branching ratio of $h \to \tau^+\tau^-$ exceeds the experimental bound. So, most of the negative $s_{\beta-\alpha}$ region is removed. The "arm" region in type X, which appears for $s_{\beta-\alpha} > 0$, is also explained by Eq. (18). When $t_\beta \simeq 2/c_{\beta-\alpha}$, ξ_τ^h approaches -1 for $s_{\beta-\alpha} \simeq 1$. We have the wrong-sign Yukawa coupling for the tau lepton.

B. Type II and type Y

We first point out that the allowed parameter points at each step in type II are almost the same as those in type Y. So, all the results in this subsection are common for type II and type Y. In type II and type Y with the CDF m_W, the biggest impact comes from the condition of $\Lambda_c > 1$ TeV. Figure 8 shows ΔM_A versus ΔM_H at Step (ii) in the left panel, at Step (iii) in the middle panel, and at Step (iv) in the right panel. The left panel shows that the oblique parameters of $S_{\rm CDF}$ and $T_{\rm CDF}$ permit the hyperbola shape with a sufficiently large mass gaps.[4] Imposing $\Lambda_c > 1$ TeV (middle panel) excludes a large portion of the parameter space, particularly with $|\Delta M_{H,A}| \gtrsim 200$ GeV. It is because too large mass gaps invoke fast running of the quartic couplings, resulting in the failure of the unitarity and vacuum stability at the energy scale below 1 TeV. The area near the mass degeneracy of $M_H = M_A = M_{H^\pm}$ is also removed. Lastly, the constraints from the collider data do not considerably change ΔM_A versus ΔM_H.

[3]Note that negative $s_{\beta-\alpha}$ in our scheme corresponds to negative $c_{\beta-\alpha}$ in the positive $s_{\beta-\alpha}$ scheme.

[4]The negative $\Delta M_{H,A}$ region is different from Fig. 1, because we assumed the Higgs alignment limit only in Fig. 1.

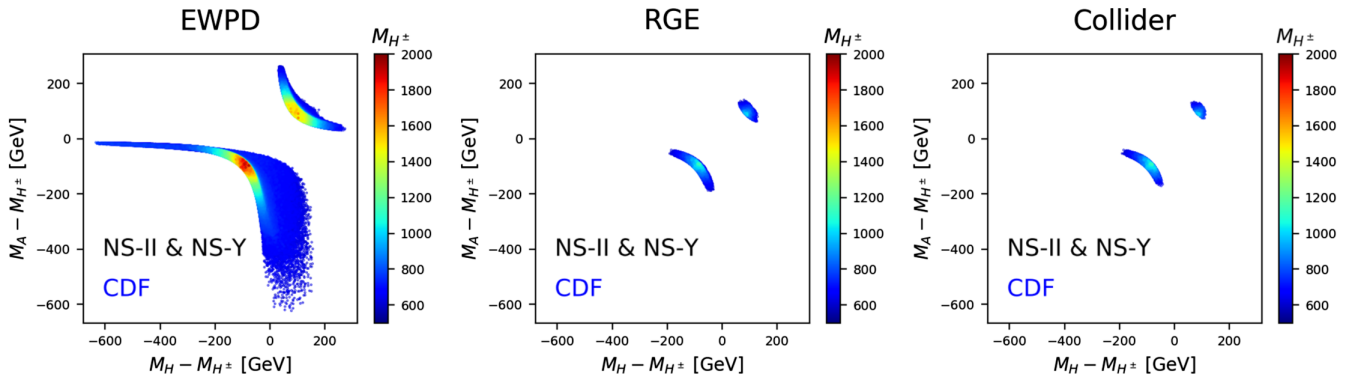

FIG. 8. In type II and type Y of the normal scenario, the allowed parameter points of $(\Delta M_H, \Delta M_A)$ at Step (ii) in the left panel, at Step (iii) in the middle panel, and at Step (iv) in the right panel, where $\Delta m \equiv m - M_{H^\pm}$. The color code denotes $M_{H^\pm}$.

Finally, let us discuss the constraint from $b \to s\gamma$. In the main analysis, we took a conservative bound on the charged Higgs boson mass as $M_{H^\pm} > 580$ GeV in type II and type Y. But the bound considerably increases to about 800 GeV if we adopt the calculation of the NNLO QCD corrections to $\mathrm{Br}(\bar{B} \to X_s\gamma)$ in the SM without the interpolation in the charm quark mass [133]. The stronger condition on $M_{H^\pm}$ restricts the other model parameters further. Focusing on $M_{H^\pm} > 800$ GeV, we additionally generated parameter points. Figure 9 presents M_A versus M_H in the left panel, and t_β versus $|s_{\beta-\alpha}|$ in the right panel, for $M_{H^\pm} > 800$ GeV. The color code indicates $M_{H^\pm}$. The lower bounds on M_H and M_A increase into about 670 GeV. Although they are smaller than the lower bound on $M_{H^\pm}$, the heavy masses of the BSM Higgs bosons make it challenging to probe NS-II or NS-Y at the HL-LHC. The right panel in Fig. 9 exhibits that the constraints on $|s_{\beta-\alpha}|$ and t_β are stronger for $M_{H^\pm} > 800$ GeV. The Higgs alignment is almost exact and the value of t_β is intermediate like $\in [0.9, 6.4]$.

V. CHARACTERISTIC FEATURES OF THE INVERTED SCENARIO

The IS accommodates a light Higgs boson at a mass below 125 GeV. This exotic scenario has drawn a lot of interest since it satisfies the theoretical requirements and the experimental data. However, the RGE analysis changes this conclusion, which has not yet been performed for the IS. According to our RGE study, type II and type Y in the IS do not retain the stability of the scalar potential up to 1 TeV, which are excluded by the condition of $\Lambda_c > 1$ TeV. In this section, therefore, we investigate the characteristics of the finally allowed parameter points of type I and type X in the CDF case.

The first remarkable feature is considerably different survival percentages between type I and type X

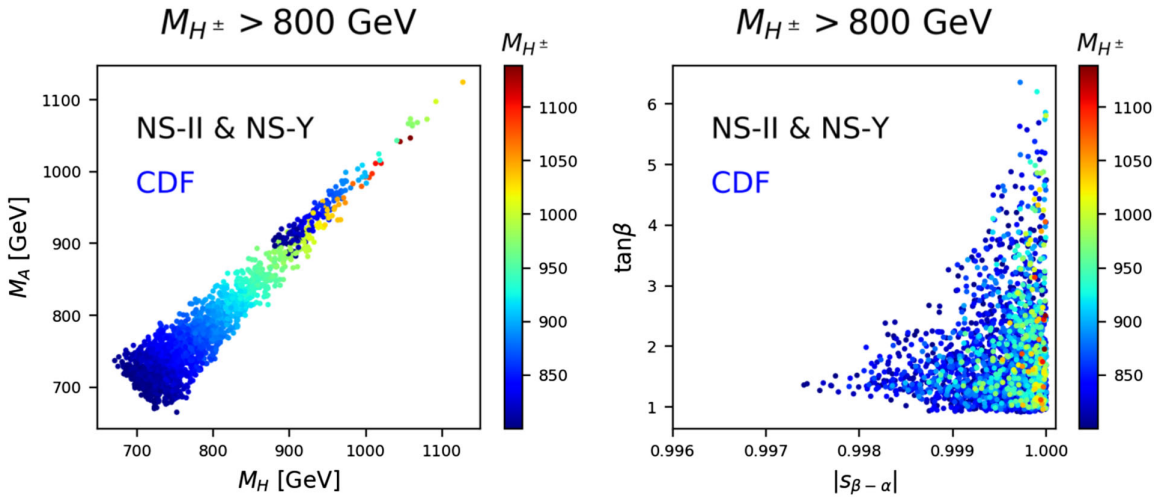

FIG. 9. For type II in the normal scenario with $M_{H^\pm} > 800$ GeV, the allowed parameter points of (M_H, M_A) in the left panel and $(|s_{\beta-\alpha}|, t_\beta)$ in the right panel. The color code denotes $M_{H^\pm}$.

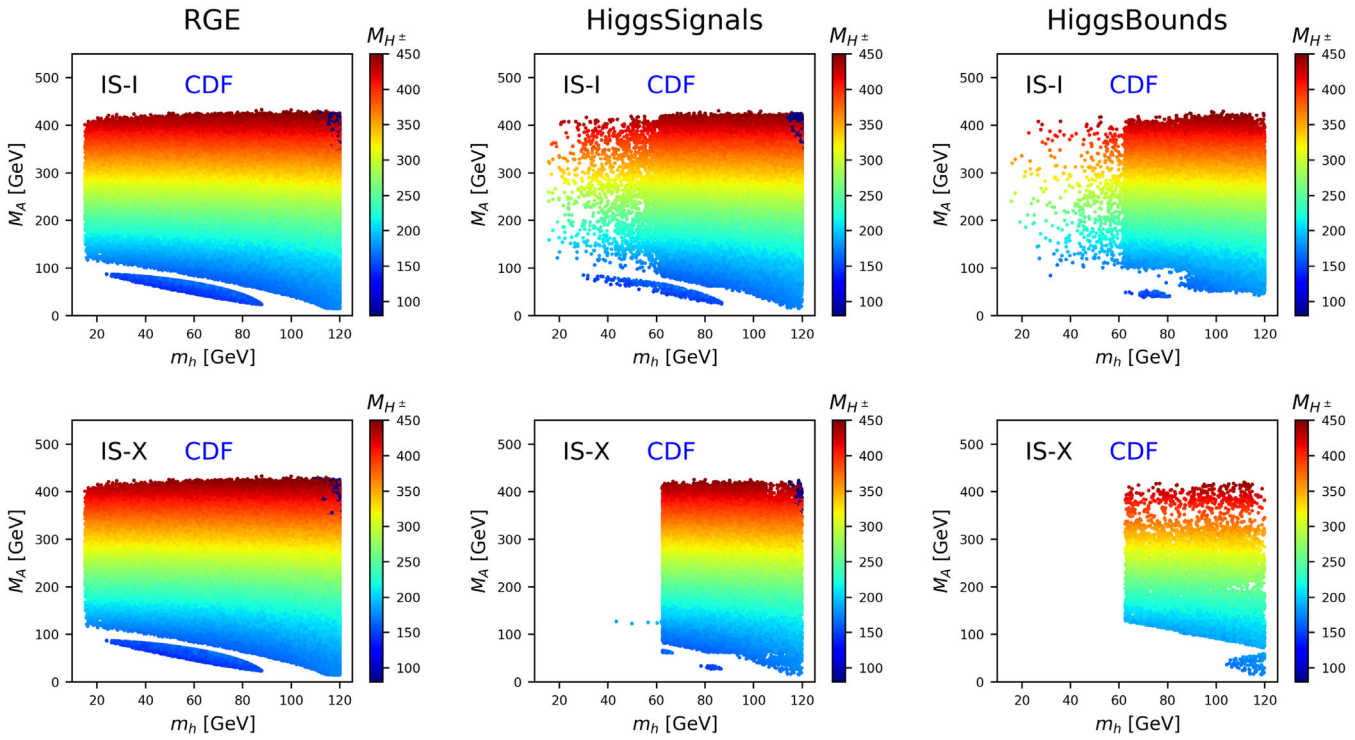

FIG. 10. Allowed parameter points of (m_h, M_A) after imposing $\Lambda_c > 1$ TeV (left panels), the Higgs precision data (middle panels), and the direct search bounds (right panels) for type I (upper panels) and type X (lower panels) in the inverted scenario. The color code denotes $M_{H^\pm}$.

(see Table II). In type X, only about 0.01% of the parameter points at Step (i) are finally allowed, but in type I, the number is 0.19%. To find the origin, we show, in Fig. 10, M_A versus m_h at the steps of $\Lambda_c > 1$ TeV (left panels), the Higgs precision data (middle panels), and the direct search bounds (right panels). The results of type I are in the upper panels and those of type X are in the lower panels. At the RGE step, type I and type X yield almost the same results. A significant difference arises after imposing the Higgs precision data. In type X, most of the parameter points with $m_h \lesssim 62.5$ GeV are excluded unlike in type I. The direct search bounds further widen the difference between type I and type X. The leptophilic nature of type X, being more severe for large t_β, brings out the severe restriction.

The second noteworthy feature in Fig. 10 is that type I permits $m_h < m_{125}/2$, but type X does not. This is due to the different decay modes of the light h in type I and type X. In type I where the ratios of the Yukawa couplings of h are the same as in the SM, the light h dominantly decays into a pair of b quarks with the branching ratio of about 80%. Since the searches for a light Higgs boson at the LHC make use of the 4τ and $2\mu 2\tau$ states [129–131], type I is less constrained. On the contrary, h in type X decays dominantly into $\tau^+\tau^-$, which is strongly limited from the $4\tau/2\mu 2\tau$ final states.

Another important result in the IS with the CDF m_W is the strong correlation among M_A, m_h, and $M_{H^\pm}$. Figure 11 shows ΔM_A versus Δm_h with a color code of $M_{H^\pm}$ for IS-I, which is similar to IS-X. We first notice that the IS in the CDF case allows only the negative Δm_h and the negative ΔM_A. It is to be compared with the NS in the CDF case, which also permits $\Delta m_h > 0$ and $\Delta M_A > 0$ (see Fig. 8). The sign of ΔM_A has a big impact on the bosonic decays

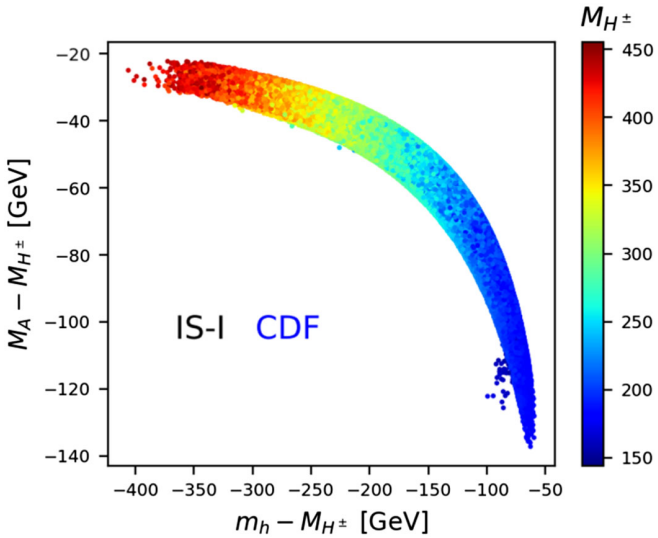

FIG. 11. Allowed parameter points of $(\Delta m_h, \Delta M_A)$ at the final step for type I in the inverted scenario, with a color code of $M_{H^\pm}$.

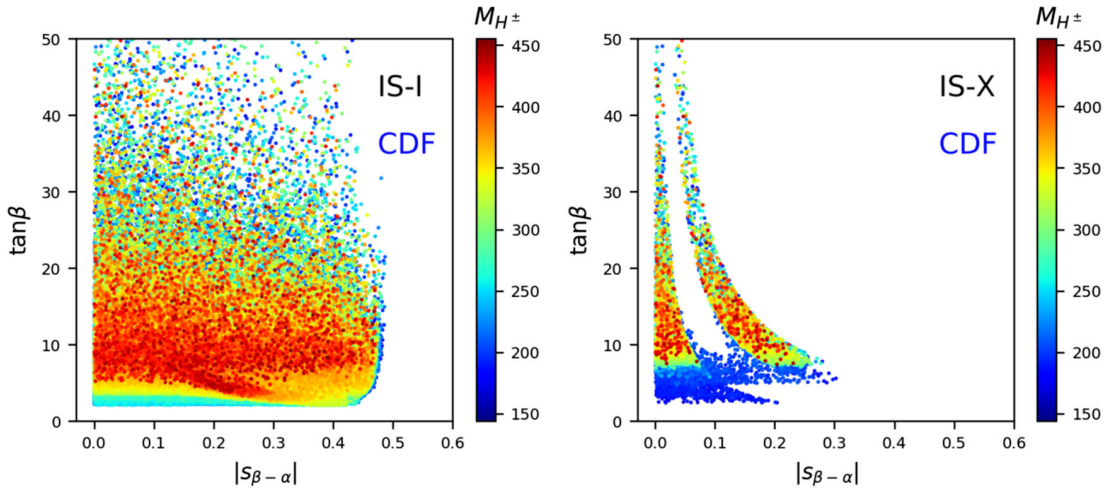

FIG. 12. Allowed parameter points of $(|s_{\beta-\alpha}|, t_\beta)$ at the final step for type I (left panel) and type X (right panel) in the inverted scenario, with a color code of $M_{H^\pm}$.

of the BSM Higgs bosons [128,134–138]. Since the charged Higgs boson is heavier than the pseudoscalar, $H^\pm \to AW^{\pm(*)}$ is feasible but $A \to H^\pm W^{\mp(*)}$ is not. Another intriguing aspect is the approximate mass degeneracy of $M_{H^\pm} \simeq M_A$ for heavy $M_{H^\pm}$; if $M_{H^\pm} \gtrsim 350$ GeV, $|\Delta M_A| < 40$ GeV. We expect that this region is very difficult to probe at the LHC. Pair productions of AH, $AH^\pm$, and H^+H^- has kinematic suppression by heavy masses. The gluon fusion production of A through the top-quark loop is also suppressed by the heavy M_A. In the large t_β limit, the cross section is further reduced because the Yukawa coupling of the top quark to A is inversely proportional to t_β. In addition, the bosonic decay mode of $H^\pm$ accompanies the soft fermions from the off shell W.

Finally, we present t_β versus $|s_{\beta-\alpha}|$ in Fig. 12 for IS-I (left panel) and IS-X (right panel) for the CDF case. The difference between type I and type X is considerable. In type I, a sizable deviation from the Higgs alignment limit is feasible. The value of $|s_{\beta-\alpha}|$ can be as large as about 0.48. In addition, large t_β around 50 is also permitted, irrespective of $s_{\beta-\alpha}$. In type X, $|s_{\beta-\alpha}| \lesssim 0.3$: the maximum deviation from the Higgs alignment is smaller than that in type I. In addition, $|s_{\beta-\alpha}|$ and t_β are more strongly correlated: if $|s_{\beta-\alpha}| = 0.3$, t_β is almost fixed to be 5.5.

VI. CONCLUSIONS

The recent W-boson mass measurement by the CDF Collaboration has a significant impact on new physics models. The central values of the Peskin-Takeuchi parameters of S and T shift to larger values; $S = 0.15 \pm 0.08$ and $T = 0.27 \pm 0.06$ with $U = 0$. In the framework of the two-Higgs-doublet model, we have studied the effects of the CDF m_W measurement together with other constraints, which include theoretical requirements (potential bounded from below, unitarity, perturbativity, vacuum stability), flavor-changing neutral currents in B physics, the cutoff scale above 1 TeV, Higgs precision data, and direct collider search limits from the LEP, Tevatron, and LHC. Pursuing the comprehensive and comparative study, we consider 16 cases, type I, type II, type X, and type Y for the normal and inverted Higgs scenarios before and after the CDF m_W measurement. The still-valid parameter space has been illustrated. The most unprecedented consequence is the upper bounds on the masses of the heavy Higgs boson $M_{H,A,H^\pm} \lesssim 1.1$ TeV in the normal scenario and $M_{H^\pm(A)} \lesssim 450\,(420)$ GeV in the inverted scenario. Such interesting findings imply that the upcoming LHC run can readily close out a significant portion of the still available parameter space.

Before closing, a few more findings from our study are offered as follows:

(1) The updated fit on the oblique parameters of S and T indicates that the new m_W measurement requires larger mass splittings among the isospin components in multiplet models.

(2) In subsequent steps of imposing constraints on the parameters, we found that the survival percentages in the CDF case are much smaller than those in the PDG case, thus implying more restriction on physics beyond the SM (not only for 2HDM). This behavior has been demonstrated in all four types and two Higgs scenarios of the 2HDM.

(3) The $\tan\beta$ is bounded from above more severely when the new $m_W^{\rm CDF}$ value is used in the normal scenario: $\tan\beta \lesssim 45, 8, 43, 17$ for type I, II, X, and Y, respectively. On the other hand, $\tan\beta$ is not bounded in type I and type X in the inverted scenario. There is no parameter space satisfying all the requirements in type II and type Y of the inverted scenario.

(4) If we raise the cutoff scale Λ_c beyond 1 TeV, the restriction on the parameter space would become more severe.

ACKNOWLEDGMENTS

We would like to thank Dr. Jin-Hwan Cho of National Institute for Mathematical Sciences in Korea for helping the numerical computation. K. C. was supported by MoST with Grant No. MOST-110-2112-M-017-MY3. The work of J. K., S. L, and J. S., is supported by the National Research Foundation of Korea, Grant No. NRF-2022R1A2C1007583.

[1] T. Aaltonen *et al.* (CDF Collaboration), High-precision measurement of the W boson mass with the CDF II detector, Science **376**, 170 (2022).
[2] P. A. Zyla *et al.* (Particle Data Group), Review of particle physics, Prog. Theor. Exp. Phys. **2020**, 083C01 (2020).
[3] S. Schael *et al.* (ALEPH, DELPHI, L3, OPAL, and LEP Electroweak Collaborations), Electroweak measurements in electron-positron collisions at W-boson-pair energies at LEP, Phys. Rep. **532**, 119 (2013).
[4] R. Aaij *et al.* (LHCb Collaboration), Measurement of the W boson mass, J. High Energy Phys. 01 (2022) 036.
[5] M. Aaboud *et al.* (ATLAS Collaboration), Measurement of the W-boson mass in pp collisions at $\sqrt{s} = 7$ TeV with the ATLAS detector, Eur. Phys. J. C **78**, 110 (2018).
[6] V. M. Abazov *et al.* (D0 Collaboration), Measurement of the W Boson Mass with the D0 Detector, Phys. Rev. Lett. **108**, 151804 (2012).
[7] M. E. Peskin and T. Takeuchi, A New Constraint on a Strongly Interacting Higgs Sector, Phys. Rev. Lett. **65**, 964 (1990).
[8] W. J. Marciano and J. L. Rosner, Atomic Parity Violation as a Probe of New Physics, Phys. Rev. Lett. **65**, 2963 (1990).
[9] D. C. Kennedy and P. Langacker, Precision Electroweak Experiments and Heavy Physics: A Global Analysis, Phys. Rev. Lett. **65**, 2967 (1990).
[10] J. Haller, A. Hoecker, R. Kogler, K. Mönig, T. Peiffer, and J. Stelzer, Update of the global electroweak fit and constraints on two-Higgs-doublet models, Eur. Phys. J. C **78**, 675 (2018).
[11] J. de Blas, M. Ciuchini, E. Franco, A. Goncalves, S. Mishima, M. Pierini, L. Reina, and L. Silvestrini, Global analysis of electroweak data in the Standard Model, Phys. Rev. D **106**, 033003 (2022).
[12] C.-T. Lu, L. Wu, Y. Wu, and B. Zhu, Electroweak precision fit and new physics in light of W boson mass, Phys. Rev. D **106**, 035034 (2022).
[13] A. Strumia, Interpreting electroweak precision data including the W-mass CDF anomaly, J. High Energy Phys. 08 (2022) 248.
[14] J. de Blas, M. Pierini, L. Reina, and L. Silvestrini, Impact of the recent measurements of the top-quark and W-boson masses on electroweak precision fits, arXiv:2204.04204.
[15] J. Fan, L. Li, T. Liu, and K.-F. Lyu, W-boson mass, electroweak precision tests and SMEFT, arXiv:2204.04805.
[16] A. Paul and M. Valli, Violation of custodial symmetry from W-boson mass measurements, Phys. Rev. D **106**, 013008 (2022).
[17] J. Gu, Z. Liu, T. Ma, and J. Shu, Speculations on the W-mass measurement at CDF, arXiv:2204.05296.
[18] P. Asadi, C. Cesarotti, K. Fraser, S. Homiller, and A. Parikh, Oblique lessons from the W mass measurement at CDF II, arXiv:2204.05283.
[19] M. Endo and S. Mishima, New physics interpretation of W-boson mass anomaly, arXiv:2204.05965.
[20] R. Balkin, E. Madge, T. Menzo, G. Perez, Y. Soreq, and J. Zupan, On the implications of positive W mass shift, J. High Energy Phys. 05 (2022) 133.
[21] L. M. Carpenter, T. Murphy, and M. J. Smylie, Changing patterns in electroweak precision with new color-charged states: Oblique corrections and the W boson mass, Phys. Rev. D **106**, 055005 (2022).
[22] M. Du, Z. Liu, and P. Nath, CDF W mass anomaly from a dark sector with a Stueckelberg-Higgs portal, Phys. Lett. B **834**, 137454 (2022).
[23] Y.-Z. Fan, T.-P. Tang, Y.-L. S. Tsai, and L. Wu, Inert Higgs Dark Matter for CDF-II W-Boson Mass and Detection Prospects, Phys. Rev. Lett. **129**, 9 (2022).
[24] C.-R. Zhu, M.-Y. Cui, Z.-Q. Xia, Z.-H. Yu, X. Huang, Q. Yuan *et al.*, GeV antiproton/gamma-ray excesses and the W-boson mass anomaly: three faces of ~60–70 GeV dark matter particle?, arXiv:2204.03767.
[25] B.-Y. Zhu, S. Li, J.-G. Cheng, R.-L. Li, and Y.-F. Liang, Using gamma-ray observation of dwarf spheroidal galaxy to test a dark matter model that can interpret the W-boson mass anomaly, arXiv:2204.04688.
[26] H. Song, W. Su, and M. Zhang, Electroweak phase transition in 2HDM under Higgs, Z-pole, and W precision measurements, arXiv:2204.05085.
[27] H. Bahl, J. Braathen, and G. Weiglein, New physics effects on the W-boson mass from a doublet extension of the SM Higgs sector, Phys. Lett. B **833**, 137295 (2022).
[28] Y. Heo, D.-W. Jung, and J. S. Lee, Impact of the CDF W-mass anomaly on two Higgs doublet model, Phys. Lett. B **833**, 137274 (2022).
[29] K. S. Babu, S. Jana, and V. P. K., Correlating W-boson mass shift with muon $g-2$ in the 2HDM, Phys. Rev. Lett. **129**, 12 (2022).
[30] T. Biekötter, S. Heinemeyer, and G. Weiglein, Excesses in the low-mass Higgs-boson search and the W-boson mass measurement, arXiv:2204.05975.
[31] Y. H. Ahn, S. K. Kang, and R. Ramos, Implications of new CDF-II W boson mass on two Higgs doublet model, arXiv:2204.06485.
[32] X.-F. Han, F. Wang, L. Wang, J. M. Yang, and Y. Zhang, A joint explanation of W-mass and muon g-2 in 2HDM, arXiv:2204.06505.

[33] G. Arcadi and A. Djouadi, The 2HD + a model for a combined explanation of the possible excesses in the CDF $\mathbf{M_W}$ measurement and $(\mathbf{g-2})_\mu$ with Dark Matter, arXiv:2204.08406.

[34] K. Ghorbani and P. Ghorbani, W-boson mass anomaly from scale invariant 2HDM, arXiv:2204.09001.

[35] A. Broggio, E. J. Chun, M. Passera, K. M. Patel, and S. K. Vempati, Limiting two-Higgs-doublet models, J. High Energy Phys. 11 (2014) 058.

[36] J. Kim, S. Lee, P. Sanyal, and J. Song, CDF W-boson mass and muon g-2 in a type-X two-Higgs-doublet model with a Higgs-phobic light pseudoscalar, Phys. Rev. D **106**, 035002 (2022).

[37] Y. Cheng, X.-G. He, Z.-L. Huang, and M.-W. Li, Type-II seesaw triplet scalar effects on neutrino trident scattering, Phys. Lett. B **831**, 137218 (2022).

[38] X. K. Du, Z. Li, F. Wang, and Y. K. Zhang, Explaining the new CDF II W-boson mass data in the Georgi-Machacek extension models, arXiv:2204.05760.

[39] S. Kanemura and K. Yagyu, Implication of the W boson mass anomaly at CDF II in the Higgs triplet model with a mass difference, Phys. Lett. B **831**, 137217 (2022).

[40] P. Mondal, Enhancement of the W boson mass in the Georgi-Machacek model, Phys. Lett. B **833**, 137357 (2022).

[41] D. Borah, S. Mahapatra, D. Nanda, and N. Sahu, Type II dirac seesaw with observable $\Delta N_{\rm eff}$ in the light of W-mass anomaly, Phys. Lett. B **833**, 137297 (2022).

[42] J. M. Yang and Y. Zhang, Low energy SUSY confronted with new measurements of W-boson mass and muon g-2, Sci. Bull. **67**, 1430 (2022).

[43] X. K. Du, Z. Li, F. Wang, and Y. K. Zhang, Explaining the muon $g-2$ anomaly and new CDF II W-boson mass in the framework of (extra)ordinary gauge mediation, arXiv:2204.04286.

[44] T.-P. Tang, M. Abdughani, L. Feng, Y.-L. S. Tsai, J. Wu, and Y.-Z. Fan, NMSSM neutralino dark matter for W-boson mass and muon $g-2$ and the promising prospect of direct detection, arXiv:2204.04356.

[45] P. Athron, M. Bach, D. H. J. Jacob, W. Kotlarski, D. Stöckinger, and A. Voigt, Precise calculation of the W boson pole mass beyond the standard model with flexibleSUSY, arXiv:2204.05285.

[46] M.-D. Zheng, F.-Z. Chen, and H.-H. Zhang, The $W\ell\nu$-vertex corrections to W-boson mass in the R-parity violating MSSM, arXiv:2204.06541.

[47] A. Ghoshal, N. Okada, S. Okada, D. Raut, Q. Shafi, and A. Thapa, Type III seesaw with R-parity violation in light of m_W (CDF), arXiv:2204.07138.

[48] P. Athron, A. Fowlie, C.-T. Lu, L. Wu, Y. Wu, and B. Zhu, The W boson mass and muon $g-2$: Hadronic uncertainties or new physics?, arXiv:2204.03996.

[49] K. Cheung, W.-Y. Keung, and P.-Y. Tseng, Isodoublet vector leptoquark solution to the muon g-2, RK,K*, RD, D*, and W-mass anomalies, Phys. Rev. D **106**, 015029 (2022).

[50] A. Bhaskar, A. A. Madathil, T. Mandal, and S. Mitra, Combined explanation of W-mass, muon $g-2$, $R_{K^{(*)}}$ and $R_{D^{(*)}}$ anomalies in a singlet-triplet scalar leptoquark model, arXiv:2204.09031.

[51] M. Blennow, P. Coloma, E. Fernández-Martínez, and M. González-López, Right-handed neutrinos and the CDF II anomaly, arXiv:2204.04559.

[52] F. Arias-Aragón, E. Fernández-Martínez, M. González-López, and L. Merlo, Dynamical minimal flavour violating inverse seesaw, J. High Energy Phys. 09 (2022) 210.

[53] X. Liu, S.-Y. Guo, B. Zhu, and Y. Li, Correlating gravitational waves with W-boson Mass, FIMP dark matter, and majorana seesaw mechanism, Sci. Bull. **67**, 1437 (2022).

[54] T. A. Chowdhury, J. Heeck, S. Saad, and A. Thapa, W boson mass shift and muon magnetic moment in the Zee model, Phys. Rev. D **106**, 035004 (2022).

[55] O. Popov and R. Srivastava, The triplet dirac seesaw in the view of the recent CDF-II W mass anomaly, arXiv:2204.08568.

[56] A. Batra, S. K. A, S. Mandal, H. Prajapati, and R. Srivastava, CDF-II W boson mass anomaly in the canonical scotogenic neutrino-dark matter model, arXiv:2204.11945.

[57] H. M. Lee and K. Yamashita, A model of vector-like leptons for the muon $g-2$ and the W boson mass, Eur. Phys. J. C **82**, 661 (2022).

[58] J. Kawamura, S. Okawa, and Y. Omura, W boson mass and muon g-2 in a lepton portal dark matter model, Phys. Rev. D **106**, 015005 (2022).

[59] A. Crivellin, M. Kirk, T. Kitahara, and F. Mescia, Correlating $t \to cZ$ to the W mass and B physics with vector-like quarks, Phys. Rev. D **106**, L031704 (2022).

[60] K. I. Nagao, T. Nomura, and H. Okada, A model explaining the new CDF II W boson mass linking to muon $g-2$ and dark matter, arXiv:2204.07411.

[61] J. Cao, L. Meng, L. Shang, S. Wang, and B. Yang, Interpreting the W mass anomaly in the vector-like quark models, Phys. Rev. D **106**, 055042 (2022).

[62] E. Bagnaschi, J. Ellis, M. Madigan, K. Mimasu, V. Sanz, and T. You, SMEFT analysis of m_W, J. High Energy Phys. 08 (2022) 308.

[63] L. Di Luzio, R. Gröber, and P. Paradisi, Higgs physics confronts the M_W anomaly, Phys. Lett. B **832**, 137250 (2022).

[64] V. Cirigliano, W. Dekens, J. de Vries, E. Mereghetti, and T. Tong, Beta-decay implications for the W-boson mass anomaly, Phys. Rev. D **106**, 075001 (2022).

[65] G.-W. Yuan, L. Zu, L. Feng, Y.-F. Cai, and Y.-Z. Fan, Hint on new physics from the W-boson mass excess-axion-like particle, dark photon or Chameleon dark energy, arXiv:2204.04183.

[66] G. Cacciapaglia and F. Sannino, The W boson mass weighs in on the non-standard Higgs, Phys. Lett. B **832**, 137232 (2022).

[67] K. Sakurai, F. Takahashi, and W. Yin, Singlet extensions and W boson mass in the light of the CDF II result, Phys. Lett. B **833**, 137324 (2022).

[68] J. J. Heckman, Extra W-boson mass from a D3-Brane, Phys. Lett. B **833**, 137387 (2022).

[69] N. V. Krasnikov, Nonlocal generalization of the SM as an explanation of recent CDF result, arXiv:2204.06327.

[70] Z. Péli and Z. Trócsányi, Vacuum stability and scalar masses in the superweak extension of the standard model, Phys. Rev. D **106**, 055045 (2022).

[71] P. Fileviez Perez, H. H. Patel, and A. D. Plascencia, On the W-mass and new Higgs bosons, Phys. Lett. B **833**, 137371 (2022).

[72] R. A. Wilson, A toy model for the W/Z mass ratio, arXiv:2204.07970.

[73] K.-Y. Zhang and W.-Z. Feng, Explaining W boson mass anomaly and dark matter with a $U(1)$ dark sector, arXiv:2204.08067.

[74] B. Abi *et al.* (Muon g-2 Collaboration), Measurement of the Positive Muon Anomalous Magnetic Moment to 0.46 ppm, Phys. Rev. Lett. **126**, 141801 (2021).

[75] A. Arbey, F. Mahmoudi, O. Stal, and T. Stefaniak, Status of the charged Higgs boson in two Higgs doublet models, Eur. Phys. J. C **78**, 182 (2018).

[76] M. Misiak and M. Steinhauser, Weak radiative decays of the B meson and bounds on $M_{H^\pm}$ in the Two-Higgs-Doublet Model, Eur. Phys. J. C **77**, 201 (2017).

[77] G. C. Branco, P. M. Ferreira, L. Lavoura, M. N. Rebelo, M. Sher, and J. P. Silva, Theory and phenomenology of two-Higgs-doublet models, Phys. Rep. **516**, 1 (2012).

[78] S. L. Glashow and S. Weinberg, Natural conservation laws for neutral currents, Phys. Rev. D **15**, 1958 (1977).

[79] E. A. Paschos, Diagonal neutral currents, Phys. Rev. D **15**, 1966 (1977).

[80] J. Song and Y. W. Yoon, $W\gamma$ decay of the elusive charged Higgs boson in the two-Higgs-doublet model with vector-like fermions, Phys. Rev. D **100**, 055006 (2019).

[81] S. Chang, S. K. Kang, J.-P. Lee, and J. Song, Higgs potential and hidden light Higgs scenario in two Higgs doublet models, Phys. Rev. D **92**, 075023 (2015).

[82] A. Jueid, J. Kim, S. Lee, and J. Song, Type-X two-Higgs-doublet model in light of the muon g-2: Confronting Higgs boson and collider data, Phys. Rev. D **104**, 095008 (2021).

[83] D. Eriksson, J. Rathsman, and O. Stal, 2HDMC: Two-Higgs-doublet model calculator physics and manual, Comput. Phys. Commun. **181**, 189 (2010).

[84] P. Bechtle, S. Heinemeyer, T. Klingl, T. Stefaniak, G. Weiglein, and J. Wittbrodt, HiggsSignals-2: Probing new physics with precision Higgs measurements in the LHC 13 TeV era, Eur. Phys. J. C **81**, 145 (2021).

[85] P. Bechtle, D. Dercks, S. Heinemeyer, T. Klingl, T. Stefaniak, G. Weiglein, and Jonas Wittbrodt, HiggsBounds-5: Testing Higgs sectors in the LHC 13 TeV era, Eur. Phys. J. C **80**, 1211 (2020).

[86] D. Das and I. Saha, Search for a stable alignment limit in two-Higgs-doublet models, Phys. Rev. D **91**, 095024 (2015).

[87] N. Chakrabarty, U. K. Dey, and B. Mukhopadhyaya, High-scale validity of a two-Higgs doublet scenario: A study including LHC data, J. High Energy Phys. 12 (2014) 166.

[88] D. Chowdhury and O. Eberhardt, Global fits of the two-loop renormalized two-Higgs-doublet model with soft Z_2 breaking, J. High Energy Phys. 11 (2015) 052.

[89] E. Bagnaschi, F. Brümmer, W. Buchmüller, A. Voigt, and G. Weiglein, Vacuum stability and supersymmetry at high scales with two Higgs doublets, J. High Energy Phys. 03 (2016) 158.

[90] P. Ferreira, H. E. Haber, and E. Santos, Preserving the validity of the two-Higgs doublet model up to the Planck scale, Phys. Rev. D **92**, 033003 (2015).

[91] N. Chakrabarty and B. Mukhopadhyaya, High-scale validity of a two Higgs doublet scenario: Metastability included, Eur. Phys. J. C **77**, 153 (2017).

[92] V. Cacchio, D. Chowdhury, O. Eberhardt, and C. W. Murphy, Next-to-leading order unitarity fits in Two-Higgs-Doublet models with soft $\mathbb{Z}_2$ breaking, J. High Energy Phys. 11 (2016) 026.

[93] D. Chowdhury and O. Eberhardt, Update of global two-Higgs-doublet model fits, J. High Energy Phys. 05 (2018) 161.

[94] N. Chakrabarty and B. Mukhopadhyaya, High-scale validity of a two Higgs doublet scenario: Predicting collider signals, Phys. Rev. D **96**, 035028 (2017).

[95] P. Basler, P. M. Ferreira, M. Mühlleitner, and R. Santos, High scale impact in alignment and decoupling in two-Higgs doublet models, Phys. Rev. D **97**, 095024 (2018).

[96] V. Branchina, F. Contino, and P. M. Ferreira, Electroweak vacuum lifetime in two Higgs doublet models, J. High Energy Phys. 11 (2018) 107.

[97] A. Dey, J. Lahiri, and B. Mukhopadhyaya, Muon g-2 and a type-X two Higgs doublet scenario: Some studies in high-scale validity, Phys. Rev. D **106**, 055023 (2022).

[98] J. Kim, S. Lee, P. Sanyal, and J. Song, Fermiophobic light Higgs boson in the type-I two-Higgs-doublet model, Phys. Lett. B **834**, 137406 (2022).

[99] G. Aad *et al.* (ATLAS Collaboration), Combined measurements of Higgs boson production and decay using up to 80 fb^{-1} of proton-proton collision data at $\sqrt{s} = 13$ TeV collected with the ATLAS experiment, Phys. Rev. D **101**, 012002 (2020).

[100] I. P. Ivanov, Minkowski space structure of the Higgs potential in 2HDM, Phys. Rev. D **75**, 035001 (2007).

[101] S. Kanemura, T. Kubota, and E. Takasugi, Lee-Quigg-Thacker bounds for Higgs boson masses in a two doublet model, Phys. Lett. B **313**, 155 (1993).

[102] A. G. Akeroyd, A. Arhrib, and E.-M. Naimi, Note on tree level unitarity in the general two Higgs doublet model, Phys. Lett. B **490**, 119 (2000).

[103] A. Barroso, P. M. Ferreira, I. P. Ivanov, and R. Santos, Metastability bounds on the two Higgs doublet model, J. High Energy Phys. 06 (2013) 045.

[104] Y. S. Amhis *et al.* (HFLAV Collaboration), Averages of b-hadron, c-hadron, and τ-lepton properties as of 2018, Eur. Phys. J. C **81**, 226 (2021).

[105] H.-J. He, N. Polonsky, and S.-f. Su, Extra families, Higgs spectrum and oblique corrections, Phys. Rev. D **64**, 053004 (2001).

[106] W. Grimus, L. Lavoura, O. M. Ogreid, and P. Osland, The Oblique parameters in multi-Higgs-doublet models, Nucl. Phys. **B801**, 81 (2008).

[107] P. A. Zyla *et al.* (Particle Data Group), Review of particle physics, Prog. Theor. Exp. Phys. **2020**, 083C01 (2020).

[108] T. P. Cheng, E. Eichten, and L.-F. Li, Higgs phenomena in asymptotically free gauge theories, Phys. Rev. D **9**, 2259 (1974).

[109] H. Komatsu, Behavior of the Yukawa and the quartic scalar couplings in grand unified theories, Prog. Theor. Phys. **67**, 1177 (1982).

[110] J. Oredsson, 2HDME: Two-Higgs-doublet model evolver, Comput. Phys. Commun. **244**, 409 (2019).

[111] M. Aaboud *et al.* (ATLAS Collaboration), Search for Higgs bosons produced via vector-boson fusion and decaying into bottom quark pairs in $\sqrt{s} = 13$ TeV pp collisions with the ATLAS detector, Phys. Rev. D **98**, 052003 (2018).

[112] M. Aaboud *et al.* (ATLAS Collaboration), Measurements of gluon-gluon fusion and vector-boson fusion Higgs boson production cross-sections in the $H \to WW^* \to e\nu\mu\nu$ decay channel in pp collisions at $\sqrt{s} = 13$ TeV with the ATLAS detector, Phys. Lett. B **789**, 508 (2019).

[113] M. Aaboud *et al.* (ATLAS Collaboration), Cross-section measurements of the Higgs boson decaying into a pair of τ-leptons in proton-proton collisions at $\sqrt{s} = 13$ TeV with the ATLAS detector, Phys. Rev. D **99**, 072001 (2019).

[114] G. Aad *et al.* (ATLAS Collaboration), Higgs boson production cross-section measurements and their EFT interpretation in the 4ℓ decay channel at $\sqrt{s} = 13$ TeV with the ATLAS detector, Eur. Phys. J. C **80**, 957 (2020).

[115] A. M. Sirunyan *et al.* (CMS Collaboration), Search for $t\bar{t}H$ production in the $H \to b\bar{b}$ decay channel with leptonic $t\bar{t}$ decays in proton-proton collisions at $\sqrt{s} = 13$ TeV, J. High Energy Phys. 03 (2019) 026.

[116] A. M. Sirunyan *et al.* (CMS Collaboration), Search for the Higgs Boson Decaying to Two Muons in Proton-Proton Collisions at $\sqrt{s} = 13$ TeV, Phys. Rev. Lett. **122**, 021801 (2019).

[117] CMS Collaboration, Measurements of properties of the Higgs boson in the four-lepton final state in proton-proton collisions at $\sqrt{s} = 13$ TeV, Report No. CMS-PAS-HIG-19-001, http://cds.cern.ch/record/2668684.

[118] CMS Collaboration, Measurements of differential Higgs boson production cross sections in the leptonic WW decay mode at $\sqrt{s} = 13$ TeV, Report No. CMS-PAS-HIG-19-002, http://cds.cern.ch/record/2691268.

[119] M. Aaboud *et al.* (ATLAS Collaboration), Search for charged Higgs bosons decaying via $H^\pm \to \tau^\pm \nu_\tau$ in the $\tau +$ jets and $\tau +$ lepton final states with 36 fb^{-1} of pp collision data recorded at $\sqrt{s} = 13$ TeV with the ATLAS experiment, J. High Energy Phys. 09 (2018) 139.

[120] A. M. Sirunyan *et al.* (CMS Collaboration), Search for charged Higgs bosons in the $H^\pm \to \tau^\pm \nu_\tau$ decay channel in proton-proton collisions at $\sqrt{s} = 13$ TeV, J. High Energy Phys. 07 (2019) 142.

[121] ATLAS Collaboration, Search for a light charged Higgs boson in $t \to H^+ b$ decays, with $H^+ \to$ cb, in the lepton + jets final state in proton-proton collisions at $\sqrt{s} = 13$ TeV with the ATLAS detector, Report No. ATLAS-CONF-2021-037, http://cds.cern.ch/record/2779169.

[122] A. M. Sirunyan *et al.* (CMS Collaboration), Search for a charged Higgs boson decaying to charm and bottom quarks in proton-proton collisions at $\sqrt{s} = 8$ TeV, J. High Energy Phys. 11 (2018) 115.

[123] G. Aad *et al.* (ATLAS Collaboration), Search for a light charged Higgs boson in the decay channel $H^+ \to c\bar{s}$ in $t\bar{t}$ events using pp collisions at $\sqrt{s} = 7$ TeV with the ATLAS detector, Eur. Phys. J. C **73**, 2465 (2013).

[124] V. Khachatryan *et al.* (CMS Collaboration), Search for a light charged Higgs boson decaying to $c\bar{s}$ in pp collisions at $\sqrt{s} = 8$ TeV, J. High Energy Phys. 12 (2015) 178.

[125] A. M. Sirunyan *et al.* (CMS Collaboration), Search for a light charged Higgs boson in the $H^\pm \to$ cs channel in proton-proton collisions at $\sqrt{s} = 13$ TeV, Phys. Rev. D **102**, 072001 (2020).

[126] S. Chatrchyan *et al.* (CMS Collaboration), Search for new physics in events with same-sign dileptons and jets in pp collisions at $\sqrt{s} = 8$ TeV, J. High Energy Phys. 01 (2014) 163.

[127] N. Craig, J. Hajer, Y.-Y. Li, T. Liu, and H. Zhang, Heavy Higgs bosons at low $\tan\beta$: From the LHC to 100 TeV, J. High Energy Phys. 01 (2017) 018.

[128] K. Cheung, A. Jueid, J. Kim, S. Lee, C.-T. Lu, and J. Song, Comprehensive study of the light charged Higgs boson in the type-I two-Higgs-doublet model, Phys. Rev. D **105**, 095044 (2022).

[129] A. M. Sirunyan *et al.* (CMS Collaboration), Search for light pseudoscalar boson pairs produced from decays of the 125 GeV Higgs boson in final states with two muons and two nearby tracks in pp collisions at $\sqrt{s} = 13$ TeV, Phys. Lett. B **800**, 135087 (2020).

[130] V. Khachatryan *et al.* (CMS Collaboration), Search for light bosons in decays of the 125 GeV Higgs boson in proton-proton collisions at $\sqrt{s} = 8$ TeV, J. High Energy Phys. 10 (2017) 076.

[131] A. M. Sirunyan *et al.* (CMS Collaboration), Search for an exotic decay of the Higgs boson to a pair of light pseudoscalars in the final state of two muons and two τ leptons in proton-proton collisions at $\sqrt{s} = 13$ TeV, J. High Energy Phys. 11 (2018) 018.

[132] S. Schael *et al.* (ALEPH, DELPHI, L3, OPAL, LEP Working Group for Higgs Boson Searches Collaborations), Search for neutral MSSM Higgs bosons at LEP, Eur. Phys. J. C **47**, 547 (2006).

[133] M. Misiak, A. Rehman, and M. Steinhauser, Towards $\bar{B} \to X_s\gamma$ at the NNLO in QCD without interpolation in m_c, J. High Energy Phys. 06 (2020) 175.

[134] A. Arhrib, R. Benbrik, R. Enberg, W. Klemm, S. Moretti, and S. Munir, Identifying a light charged Higgs boson at the LHC Run II, Phys. Lett. B **774**, 591 (2017).

[135] T. Mondal and P. Sanyal, Same sign trilepton as signature of charged Higgs in two Higgs doublet model, J. High Energy Phys. 05 (2022) 040.

[136] S. Kanemura, K. Tsumura, and H. Yokoya, Multi-tau-lepton signatures at the LHC in the two Higgs doublet model, Phys. Rev. D **85**, 095001 (2012).

[137] A. Arhrib, R. Benbrik, M. Krab, B. Manaut, S. Moretti, Y. Wang, and Q.-S. Yan, New discovery modes for a light charged Higgs boson at the LHC, J. High Energy Phys. 10 (2021) 073.

[138] A. Arhrib, R. Benbrik, M. Krab, B. Manaut, S. Moretti, Y. Wang *et al.*, New light H± discovery channels at the LHC, Symmetry **13**, 2319 (2021).